Research paper

Structure-based design, synthesis and evaluation of a novel family of PEX5-PEX14 interaction inhibitors against *Trypanosoma*

Valeria Napolitano [a,b,1,**], Piotr Mróz [c], Monika Marciniak [c], Vishal C. Kalel [d], Charlotte A. Softley [e,f], Julian D. Janna Olmos [a], Bettina G. Tippler [d], Kenji Schorpp [g], Sarah Rioton [e,f], Tony Fröhlich [e,f], Oliver Plettenburg [h], Kamyar Hadian [g], Ralf Erdmann [d], Michael Sattler [e,f], Grzegorz M. Popowicz [e,f], Maciej Dawidowski [c,***], Grzegorz Dubin [a,b,*]

[a] *Malopolska Centre of Biotechnology, Jagiellonian University, Gronostajowa 7a, 30-387, Krakow, Poland*
[b] *Faculty of Biochemistry, Biophysics and Biotechnology, Jagiellonian University, Gronostajowa 7, 30-387, Krakow, Poland*
[c] *Department of Drug Technology and Pharmaceutical Biotechnology, Faculty of Pharmacy, Medical University of Warsaw, Banacha 1, 02-097, Warsaw, Poland*
[d] *Institute of Biochemistry and Pathobiochemistry, Department of Systems Biochemistry, Faculty of Medicine, Ruhr University Bochum, Universitätsstrasse 150, 44801, Bochum, Germany*
[e] *Institute of Structural Biology, Helmholtz Zentrum München, Ingolstädter Landstrasse 1, D-85764, Neuherberg, Germany*
[f] *Center for Integrated Protein Science Munich at Chair of Biomolecular NMR, Department of Chemistry, Technical University of Munich, Lichtenbergstrasse 4, 85747 Garching, Germany*
[g] *Institute of Molecular Toxicology and Pharmacology, Helmholtz Zentrum München, Ingolstädter Landstrasse 1, D-85764, Neuherberg, Germany*
[h] *Institute of Medicinal Chemistry, Helmholtz Zentrum München, Ingolstädter Landstrasse 1, D-85764, Neuherberg, Germany*

ARTICLE INFO

ABSTRACT

Trypanosomiases are neglected tropical diseases caused by *Trypanosoma* (sub)species. Available treatments are limited and have considerable adverse effects and questionable efficacy in the chronic stage of the disease, urgently calling for the identification of new targets and drug candidates.

Recently, we have shown that impairment of glycosomal protein import by the inhibition of the PEX5-PEX14 protein-protein interaction (PPI) is lethal to *Trypanosoma*. Here, we report the development of a novel dibenzo[*b*,*f*][1,4]oxazepin-11(10*H*)-one scaffold for small molecule inhibitors of PEX5-PEX14 PPI. The initial hit was identified by a high throughput screening (HTS) of a library of compounds. A bioisosteric replacement approach allowed to replace the metabolically unstable sulphur atom from the initial dibenzo[*b*,*f*][1,4]thiazepin-11(10*H*)-one HTS hit with oxygen. A crystal structure of the hit compound bound to PEX14 surface facilitated the rational design of the compound series accessible by a straightforward chemistry for the initial structure-activity relationship (SAR) analysis. This guided the design of compounds with trypanocidal activity in cell-based assays providing a promising starting point for the development of new drug candidates to tackle trypanosomiases.

1. Introduction

Trypanosomatids are unicellular protist parasites that belong to the order of *Kinetoplastea* [1]. A number of *Trypanosoma* species are responsible for severe veterinary diseases and two species cause potentially lethal human diseases [2]. In sub-Saharan Africa, *T. brucei* infections lead to sleeping sickness or human African trypanosomiasis (HAT) [3]. In Americas, *T. cruzi* causes Chagas disease [4]. HAT and Chagas disease are neglected tropical diseases (NTDs) associated with a significant morbidity and mortality and together with related animal diseases limit the economic development in some of the poorest regions of the world [1,5,6].

Two subspecies of the uniflagellate *Trypanosoma brucei* (i.e. *T.b*

Abbreviations

PPI	protein-protein interaction	HPLC-MS	High pressure liquid chromatography mass spectrometry
HTS	high-throughput screening	HRMS	High resolution mass spectrometry
NTDs	neglected tropical diseases	ESI	electrospray ionization
SAR	structure-activity relationship	TMS	tetramethylsilane
HAT	human african trypanosomiasis	DMSO	Dimethyl sulfoxide
PEX	peroxin	s	singlet
WHO	World Health Organization	d	doublet
PTS	peroxisome targeting signal	t	triplet
TPR	tetratricopeptide repeat	q	quartet
STD	NMR Saturation Transfer Difference	dd	doublet of doublets
NTD	N-terminal domain	dt	doublet of triplets
PTM	Post-translational modification	bs	broad signal
*m*CPBA	*meta*-chloroperoxybenzoic acid	m	multiplet
DCM	dichloromethane; rt, room temperature	AEBSF	4-(2-aminoethyl)benzenesulfonyl fluoride hydrochloride
TEA	trimethylamine; DMAP, 4-dimethylaminopyridine	PBS	phosphate-buffered saline
THF	tetrahydrofuran	SEC	size exclusion chromatography
DMF	dimethylformamide	BSA	bovine serum albumin
EDC	1-Ethyl-3-(3-dimethylaminopropyl)carbodiimide	BSF	bloodstream form
DIEA	N,N-Diisopropylethylamine	FBS	fetal bovine serum
MST	Microscale thermophoresis	*Tb*PEX14	*T. brucei* PEX14 N-terminal domain
TLC	Thin Layer Chromatography	*Hs*PEX14	human PEX14 N-terminal domain
		*Tc*PEX14	*T. cruzi* PEX14 N-terminal domain

gambiense and *T.b rhodesiense*) are responsible for HAT. The disease is transmitted by the bites of the infected tsetse flies. The infection proceeds in two stages, an acute stage (Stage 1) characterized by waxing and waning flulike symptoms followed by a meningoencephalitic stage (Stage 2) after the trypanosomes pass the blood-brain barrier to infect the central nervous system [7]. If not correctly diagnosed and properly treated, HAT is almost invariantly fatal [7,8]. HAT epidemics in the 20th century [9] and resultant disease surveillance and management by World Health Organization (WHO) resulted in a steadily decreasing number of cases confined in well-defined foci of endemicity. The COVID-19 pandemic has given a stark reminder of how the process of HAT elimination can be threatened by unexpected challenges [10,11]. The World Health Organization (WHO) set new targets for HAT in its 2021–2030 road map for NTDs, namely: the elimination of transmission of *gambiense* HAT, which occurs in western and central Africa, and the elimination as a public health problem of *rhodesiense* HAT, which is found in eastern and southern Africa [10].The prospects of vaccine development against HAT are poor because *T. brucei* is able to change the antigenic character of its glycoprotein surface coat and so evade the host's immune response [12]. Current treatments for HAT include suramin and pentamidine for the acute stage of HAT, and melarsoprol, eflornithine, and nifurtimox–eflornithine combination therapy (NECT) for the chronic stage II of the disease (Fig. 1). Unfortunately, these drugs have severe side effects and require a continuous parenteral administration – a significant complication in remote areas [7,13]. In 2019, fexinidazole, the first all-oral drug for *gambiense* HAT, was included in the WHO Essential medicines list and the WHO human African Trypanosomiasis treatment guidelines. Nevertheless, given the shared mechanism of action with the other nitroaromatic drugs (e.g. nifurtimox), cross-resistance looms over fexinidazole monotherapy [14,15]. Furthermore, fexinidazole is indicated only for the first stage and non-severe second stage [16,17]. Of further development, SCYX-7158 (acoziborole) undergoes Phase 2/3 clinical evaluation as a single dose oral treatment for adult patients with *gambiense* HAT [18,19], but no alternatives are evaluated in clinics.

Around 8 million people are currently estimated to suffer from Chagas disease [20–22]. The majority live in Central and South America, and Mexico, but migration has resulted in increasing numbers of infected individuals in the formerly non-endemic areas, including Europe,

Japan, Australia, Canada, and the United States [23–25]. *T. cruzi* spreads through the bites of the hematophagous triatomine bugs and non-vectorial routes including the congenital transmission and the medical procedures (blood transfusion and organ transplants) [26,27]. The initial acute stage of the infection is usually mild or asymptomatic. The chronic stage can also be asymptomatic, but an estimate 20–30% of the subjects develop debilitating progressive cardiac and/or gastrointestinal pathologies. Chagas cardiomyopathy rapidly progresses with heart failure and high prevalence of sudden cardiac death. Only two trypanocidal drugs are currently available in Chagas disease: benznidazole and nifurtimox (Fig. 1) [28]. Both are effective only in the acute phase while their efficiency drastically drops in the chronic stage (10–40%) [29,30]. Long treatment regimens are required and the physicians are frequently forced to stop the uncompleted treatment due to the significant adverse effects [31,32]. The poor performance of the available drugs calls for the development of safer and more effective treatments. Despite being a global threat, at the moment only fexinidazole is in clinical evaluation for the short-course and the low-dose regimens in adults with chronic Chagas disease [16,33]. This calls for increased efforts in anti *T. cruzi* drug development.

Unique to trypanosomes, the first seven enzymes of the glycolytic pathway as well as the enzymes of several other important metabolic pathways [34] are compartmentalized in the glycosomes, specialized peroxisome-like organelles [35–37]. Different developmental stages of *Trypanosoma* show different level of dependence on glycolysis [38]. The bloodstream form of *T. brucei* lacks the functional Krebs cycle and the mitochondrial respiratory chain, and uses glycolysis as the only source of ATP [39,40]. *T. cruzi* is less dependent on glycolysis. It has been demonstrated that the interference in the glycosome function leads to the metabolic catastrophe and the rapid death of trypanosomes by deregulating glycolytic flux [42] and likely other glycosomes related pathways.

The biogenesis of the glycosomes and the translocation of the glycolytic enzymes is mediated by the peroxin proteins (PEX), which are thus fundamental for the survival of the parasites [43]. After being synthesized in the cytosol, the glycosomal enzymes that carry the peroxisomal targeting signal (PTS1) are recognized by PEX5 through its C-terminal tetratricopeptide repeat (TPR) domain. PEX5 also acts as a co-receptor for PEX7 which recognizes the PTS2 containing enzymes.
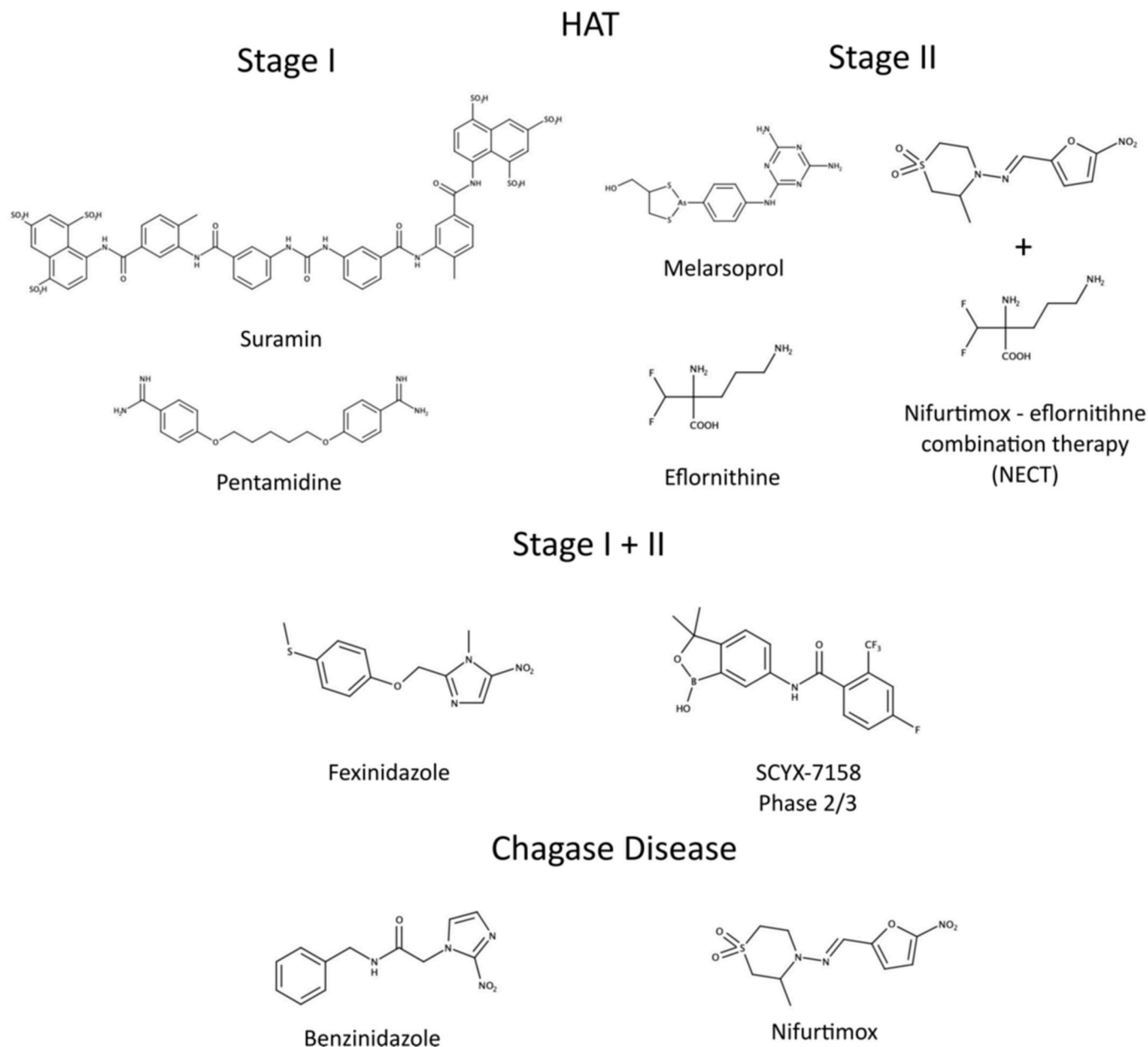
Fig. 1. The chemical structures of the drugs available against trypanosomiases.

The intrinsically disordered N-terminal domain of PEX5 contains several WxxxF motifs that allow the docking at the glycosomal membrane by binding to the N-terminal helical domain of PEX14 (Fig. 2A). The PEX5-PEX14 PPI is essential for the glycosomal protein import and has been identified as the "Achilles' heel" of *Trypanosoma*. Indeed, using the structure-based drug design, some of us developed the first small molecule inhibitors of the *Trypanosoma* PEX5-PEX14 PPI that disrupt the glycosomal protein import and kill the parasites both *in vitro* and *in vivo* [44]. The study provided a proof-of-concept that the PEX system is a valid target in trypanosomiases (Fig. 2B), but the development of efficient and safe drug-like inhibitors continues.

In this paper we report the identification and optimization of the novel dibenzo[*b,f*][1,4]thiazepin-11(10*H*)-one and dibenzo[*b,f*][1,4] oxazepin-11(10*H*)-one scaffolds for the PEX14 inhibition with trypanocidal activity. The initial hits were identified *via* a HTS of a library of compounds. We present an X-ray structure that explains the binding pose of the primary hit at the *Tc*PEX14 PEX5 binding pocket, and shows that the investigated tricyclic core of the scaffold might be generally

useful in the design of small molecular weight compounds mimicking the binding of the helical motifs. We also bypass the metabolic instability of the scaffold by bioisosteric replacement of the sulphur in the initial dibenzo[*b,f*][1,4]thiazepin-11(10*H*)-one scaffold of the HTS hit with the oxygen of the dibenzo[*b,f*][1,4]oxazepin-11(10*H*)-one scaffold. A preliminary SAR analysis is provided by the synthesis of a set of compounds, many of which demonstrate promising trypanocidal activity against *T. brucei*.

2. Results and discussion

2.1. Hit identification and structural characterization of the binding mode to PEX14

To identify small molecule inhibitors of the PEX5-PEX14 PPI we implemented an AlphaScreen [44,45] based interaction assay and screened a 30,000 molecules diversity set (ChemBridge, ChemDiv, Enamine, ChemDiv Protein-Protein Interaction (PPI)) for potential
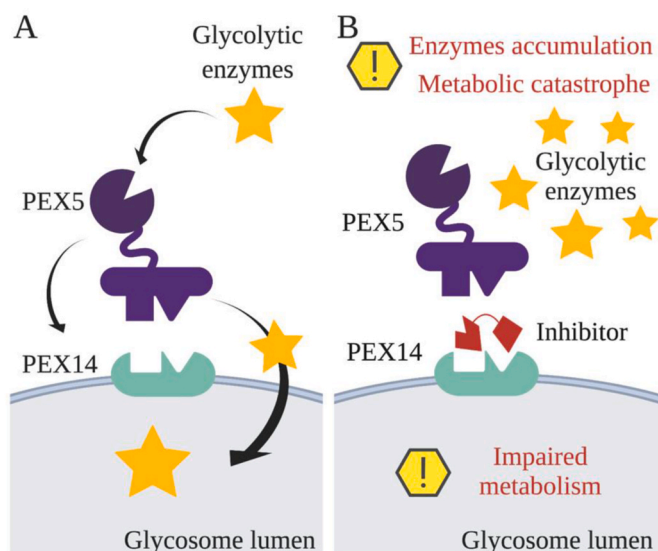
Fig. 2. A) The glycosomal protein import mechanism. Glycolytic enzymes, expressed on free ribosomes in the cytosol and which contain a PTS1 signal sequence are recognized by the PEX5 TPR domain. The cargo-PEX5 complex docks at the glycosomal membrane by binding PEX14. Together with other PEX proteins (not shown for clarity), PEX14 and PEX5 translocate glycolytic enzymes inside the glycosome where the glycolysis is compartmentalized in *Trypanosoma*. **B)** The inhibition of the glycosomal protein import. Small molecules that inhibit the PEX5-PEX14 PPI cause mislocalization of the glycolytic enzymes and a metabolic catastrophe leading to the parasite's death.

inhibitors. A number of hits were selected and re-evaluated using the NMR Saturation Transfer Difference (STD) experiment [46]. Compounds **1** and **2** passed the orthogonal evaluation for PEX14 binders and were considered further in this study (Table 1).

To facilitate the hit optimization, we screened for the crystallization conditions of compound **1** in complex with *Tb*PEX14 and *Tc*PEX14 and succeeded in the determination of the crystal structure of compound **1** in complex with the N-terminal domain (NTD) of *Tc*PEX14 (Fig. 3). The best crystal of **1**-*Tc*PEX14 complex diffracted up to 2.18 Å resolution. The crystal belonged to the *P* 1 2₁ 1 space group. The asymmetric unit contained two protein-ligand complex molecules. The three-helical bundle fold of *Tc*PEX14 revealed by our structure resembles the folds characteristic for *T. brucei* and *H. sapiens* PEX14. Compound **1** mimics the binding pose of PEX5 WxxxF motif to PEX14 (Fig. 3B) [44,47]. One of the benzene rings of the dibenzo[*b*,*f*][1,4]thiazepin-11(10*H*)-one tricyclic scaffold of compound **1** accommodates the Phe pocket and overlaps well with the phenyl group of the Phe107 residue of the PEX5 WxxxF motif. The 4-fluorophenylacetamide moiety attached to the C-7 position of the central scaffold accommodates the Trp pocket. Alike the indole group of the Trp103 residue of the PEX5 WxxxF sequence, the 4-fluorophenyl residue of compound **1** stacks between the α1 and α3 helices of *Tc*PEX14 where it is stabilized by a number of π-π and van der Waals interactions [48] (Fig. 3B). The bent structure of the central tricyclic scaffold of compound **1** allows concomitant access to the phenylalanine and tryptophan pockets and shields the hydrophobic surface of the receptor (formed by the stacked Phe35 and Phe52 residues) against the solvent. The shielding is comparable to that provided by the WxxxF helix of PEX5 (Fig. 3B). Additional interactions are mediated by a salt bridge contributed by Lys56 and an extended water network around Ser31 and Asp38 (Fig. 3C). Because of the high sequence similarity between *Tb*PEX14 and *Tc*PEX14 the structure informed not only on compound **1** binding to *Tc*PEX14, but also on the likely mode of binding to *Tb*PEX14 (for which we were unsuccessful in obtaining the crystals with compound **1**) which is of interest for the compound optimization in this study.

It is important to highlight that although the overall structure of

PEX14 is well preserved among the species, the sequence identity is below 30% between human and *Trypanosoma*. Of particular importance are the hydrophilic residues surrounding the binding pocket. These three residues are different in *Trypanosoma* (*Tb*Asn31/*Tc*Ser31, *Tb*Glu34/*Tc*Gln31, Asp38) and human (Thr31, Lys16, Asn38), and thus they might be useful for establishing the species-selectivity of the inhibitors.

To assess if the compound binding is associated with the potential receptor dynamics we superimposed the compound **1**-*Tc*PEX14 complex structure with the structure of the apo-protein (PDB code: 6ZFW [49]). The protein conformations in the two structures differ only in the distal part of the α1 helix (Figure S1) which is beyond the inhibitor binding site. This shows that no significant induced fit is involved in compound **1** binding.

2.2. Improvement of the metabolic stability of the hit scaffold by bioisosteric replacement

The visual inspection of the hit compounds **1** and **2** suggested the possible stability issues related to the sulphur atom in the heterocyclic central scaffold [50]. The *in vitro* assessment of the stability of compound **2** in the mouse liver microsomes identified a major metabolic transformation product **M8** characterized by +16 Da mass compared to the parent compound, suggesting a mono-oxidation, which was confirmed by the MS/MS analysis. In addition, minor metabolites were found including the products of the amide dealkylation (**M7**) and bis-oxidation (**M9**) (Figure S2).

To determine if the major metabolite **M8** retained the biological activity of the parent compound **2**, the metabolite was synthesized and its ability to dissociate the PEX5-PEX14 interaction was determined. The sulfoxide derivative **3** (**M8**) showed weak activity against *Tb*PEX14 in AlphaScreen, which activity was not confirmed with MST. No activity against *Tc*PEX14 in either AlphaScreen or MST assays was detected. Because of the rapid metabolic conversion of the dibenzo[*b*,*f*][1,4] thiazepin-11(10*H*)-one scaffold into an inactive oxidized product we evaluated the bioisosteric replacement of the sulphur with an oxygen atom. The resultant compound **8c** was active in inhibiting PEX5-PEX14 interaction demonstrating the success of the bioisosteric replacement strategy. More importantly, **8c** successfully killed the *T. brucei brucei* parasites in an *in vitro* assay (EC₅₀ = 8.12 μM). This encouraged us to proceed with the derivatization of the dibenzo[*b*,*f*][1,4]oxazepin-11 (10*H*)-one scaffold to obtain preliminary SAR data in this novel class of PEX14 ligands.
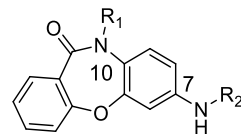
2.3. Chemistry

Compounds **1** and **2** were obtained from commercial sources. The major product of the metabolic conversion of compound **2**, the sulfoxide **3**, was obtained by the oxidation of the parent compound using *m*-CPBA as shown in Scheme 1.

ᵃReagents and conditions: (a) *m*-CPBA, DCM, rt.

The PEX14-PEX5 PPI inhibitors **8a-p** bearing various acyl moieties attached to the amine group in position C-7 of the dibenzo[*b*,*f*][1,4] oxazepin-11(10*H*)-one scaffold were synthesized as depicted in Scheme 2. The starting 2-amino-5-nitrophenol was acylated with 2-fluorobenzoyl chloride to give the anilide **4** that underwent cyclisation to the dibenzo[*b*,*f*][1,4]oxazepin-11(10*H*)-one derivative **5** upon the treatment with NaOH at the elevated temperature. The alkylation of the amide moiety in **5** gave the *N*-ethylamide **6**. The subsequent reduction of the nitro group with SnCl₂ gave the aniline **7**. Next, the *N*-acylation reactions of **7** using the carboxylic acids, (*S*)–*N*-Boc-Phg-OH or acyl chlorides, gave the respective derivatives **8a-l** and **8n-p**. The phenylglycinate derivative **8m** was obtained by the Boc-deprotection of compound **8l** in the acidic conditions.

ᵃReagents and conditions: (a) 2-fluorobenzoyl chloride, TEA, DMAP₍cat.₎, THF, 0 °C to rt; (b) NaOH, DMF, reflux; (c) NaH, DMF, then
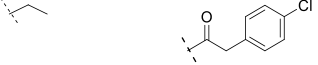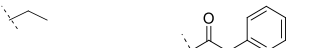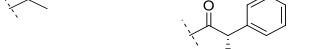
Table 1

SAR in dibenzo[*b*,*f*][1,4]oxazepin-11(10*H*)-one based PEX5-PEX14 PPI inhibitors.

#	Chemical structure	AlphaScreen		MST		*T. brucei brucei* IC$_{50}$ [μM][c]
		*Tb*PEX14 EC$_{50}$ [μM][a]	*Tc*PEX14 EC$_{50}$ [μM][a]	*Tb*PEX14 K$_d$ [μM][b]	*Tc*PEX14 K$_d$ [μM][b]	
1		230	637	951	56	5.40 (4.76–6.12)
2		1051	2291	24	5	0.86 (0.80–0.91)
3		1729	nd	nd	nd	nd

#	R$_1$	R$_2$	AlphaScreen *Tb*PEX14 EC$_{50}$ [μM]	*Tc*PEX14 EC$_{50}$ [μM]	MST *Tb*PEX14 K$_d$ [μM]	*Tc*PEX14 K$_d$ [μM]	*T. brucei brucei* IC$_{50}$ [μM][b]
8c			875	4590	131	124	8.12 (7.41–8.94)
1. Solvent-exposed region							
10			11000	551	nd	nd	20.71 (17.70–24.22)
11c			422	10265	2	3000	19.34 (17.26–21.68)
11a			7227	4590	nd	nd	11.59 (10.30–13.05)
11b			480	nd	369	258	7.70 (7.07–8.39)
2. Trp pocket							
8a			1092	788	nd	nd	13.35 (11.51–15.48)
8k			843	1229	1460	3450	29.4 (26.37–32.44)
8f			741	1928	840	nd	47.60 (41.8–54.2)
8d			500	2933	44	64	7.38 (6.43–8.48)

Table 1 (*continued*)

#	Chemical structure	AlphaScreen		MST		T. brucei brucei IC$_{50}$ [μM][c]
		TbPEX14 EC$_{50}$ [μM][a]	TcPEX14 EC$_{50}$ [μM][a]	TbPEX14 K$_d$ [μM][b]	TcPEX14 K$_d$ [μM][b]	
8e		54	2368	385	2800	5.39 (4.49–6.47)
8h		nd	nd	61000	1700	~57.5
8g		825	2362	29	9	8.30 (7.58–9.08)
8m		253	421	625	10200	13.4 (10.01–17.4)
8l		318	1611	380	2	~58.5
8n		250	3589	232	100000	~52.8
8p		3630	6834	158	252	19.4 (16.32–22.72)
8o		935	778	20	12	7.1
8i		109	677	13	9	13.7 (12.3–12.94)
8j		351	12955	14	3	7.9 (7.3–8.64)
8b		69	4516	147	42	6.35 (5.71–7.07)

[a] EC$_{50}$ values were calculated as a Hill curve fit to 12-point titration. The values are shown as mean (n = 4).
[b] K$_d$ values were calculated using MO.Affinity Analysis software. The values are shown as mean (n = 3).
[c] EC$_{50}$ values are shown as mean (n = 4). Values in parentheses are 95% confidence intervals. nd – not determined; the compound was inactive in the concentration range tested.
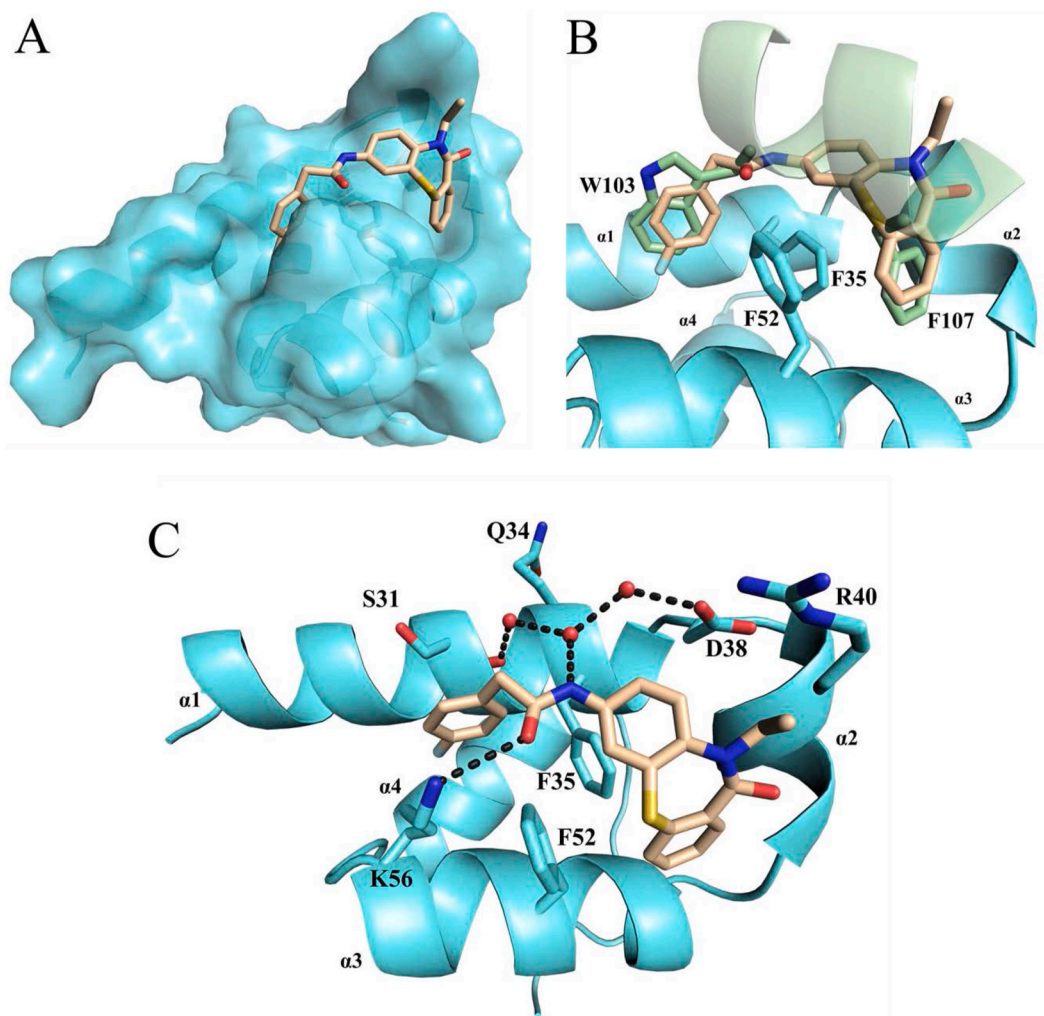
Fig. 3. A) Surface representation of *T. cruzi* NTD-PEX14 domain in complex with compound **1**. The compound fills the shallow Trp and Phe pockets of *Tc*PEX14 and covers a large hydrophobic surface of the PEX5-PEX14 PPI interface. **B)** Comparison of the binding pose of compound **1** at the binding site of *Tc*PEX14 NTD and the PEX5 WxxxF motif at the binding site of *Hs*PEX14 NTD (PDB code: 2W84 [47]). *Tc*PEX14 NTD is represented as cartoon (light blue), compound **1** in gold and the PEX5 WxxxF motif in light green. Compound **1** mimics the binding pose of the WxxxF motif of PEX5. **C)** Interactions formed by compound **1** at the PEX5-PEX14 PPI interface. The 4-fluorophenyl group is π-π stacked between the α1 and α3 helices. A salt bridge with Lys56 and two water-mediated H-bonds with Ser31 and Asp38 support the binding. The water molecules are represented as red spheres and the H-bonds as black dashed lines.

EtBr, rt; (d) SnCl$_2$, EtOH, reflux; (e) Arylacetic acid, EDC, HOBt, DIEA, DMF, rt (for **8a-k**) or *N*-Boc-L-Phg-OH, EDC, HOBt, DIEA, DMF, rt (for **8l**), or phenyl chloroformate, TEA, DMAP$_{(cat.)}$, THF, 0 °C to rt (for **8n**) or sulfonyl chloride, TEA, DMAP$_{(cat.)}$, THF, 0 °C to rt (for **8o-p**); (f) 4 N HCl in 1,4-dioxane.

The derivatives **11a-c** with various substituents in the cyclic amide group of dibenzo[*b,f*][1,4]oxazepin-11(10*H*)-one framework were obtained according to Scheme 3. The nitro derivative **5** was reduced to the corresponding aniline **9** that was then acylated with 4-fluorophenylacetic acid to give the anilide **10**. The subsequent deprotonation of the

cyclic amide in **10** followed by the *N*-alkylation or the *N*-acylation reactions gave the respective derivatives **11a-c**.

^{a}Reagents and conditions: (a) SnCl$_2$, EtOH, reflux; (b) 4-fluorophenylacetic acid, EDC, HOBt, DIEA, DMF, rt; (c) NaH, DMF, rt, then methyl bromoacetate, rt (for **11a**), or NaH, DMF, rt, then methyl chloroformate, rt (for **11b**), or NaH, DMF, rt, then methanesulfonyl chloride, rt (for **11c**).
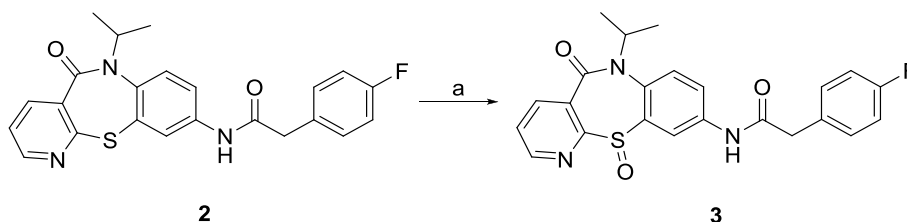
Scheme 1. Synthesis of compound **3**^{a}.
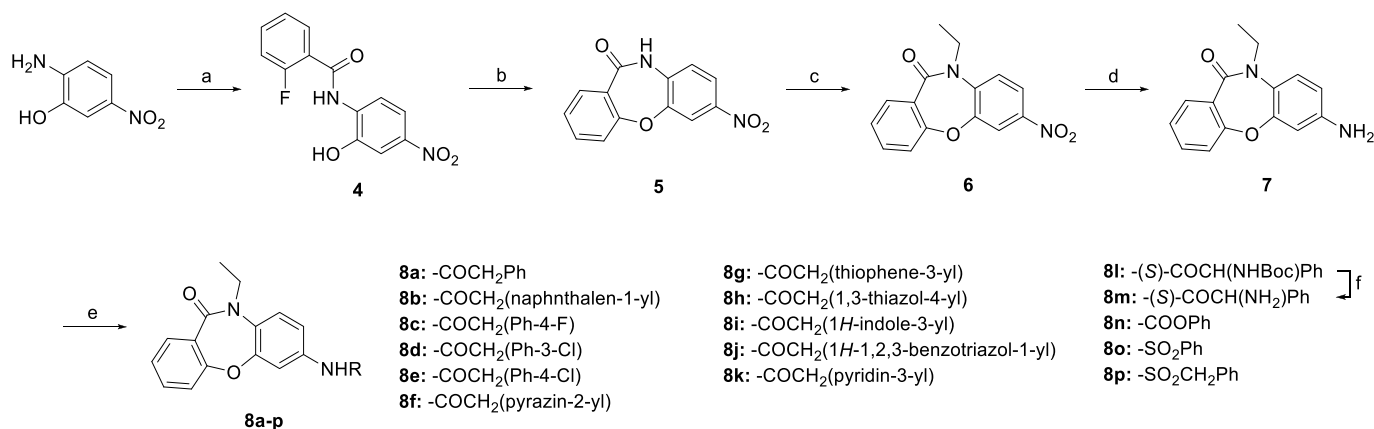
Scheme 2. Synthesis of compounds **8a-p**[a].

2.4. Structure-activity relationship (SAR)

The synthetic route to target dibenzo[*b,f*][1,4]oxazepin-11(10*H*)-ones allowed the convenient access to derivatives with various: i) cyclic amide substituents (R_1) in compounds **10,11a-c** and ii) acyl substituents at the amino group in the C-7 position in compounds **8a-p** (R_2) (Table 1). R_1 allowed to explore the solvent-exposed region of the interface. R_2 permitted the sampling of the Trp pocket which we considered more suitable for the initial SAR studies compared to the shallower and more solvent exposed Phe pocket (Fig. 3).

For the initial functional evaluation, the synthesized derivatives were tested for their ability to dissociate PEX14 interaction with the WxxxF motif encompassing peptide in the AlphaScreen assay. Following the initial assessment, the affinities (K_d) towards PEX14 were determined by Microscale Thermophoresis (MST). Significant differences in the affinities determined by the two methods were observed for certain compounds. Because both methods successfully passed the validation using known inhibitors and inactive compounds it is likely that some of the variation observed in the results reported in this study may be explained by the interference of the selected compounds with either of the assays. The two assays are based on different principles and thus differential unspecific interference of certain compounds may not be excluded. The SAR model detailed below is constructed based on the trends in the K_d and the EC_{50} values while appreciating the uncertainty of certain conclusions.

In parallel to the affinity testing, the compounds were tested for the trypanocidal activity in cell-based assay against *T. brucei brucei*.

The modifications at the cyclic amide (R_1) included the ethyl deletion in compound **10** and the changes in the type and the size of the substituent in derivatives **11a**, **11b** and **11c**. Compound **10** showed only weak affinity to *Tb*PEX14 in the AlphaScreen assay (no activity in MST) demonstrating that a substituent at the cyclic amide has an important role in the binding of the ligand to *Tb*PEX14. Different aliphatic substituents are tolerated at the R_1 position (compounds **1, 2**) presumably providing favourable interactions with the alkyl portion of the Arg40 side chain. Given the presence of the polar residues (Asp38 and Arg40) in the proximity of R_1 we tested polar substituents at this position.

Compound **11c** with a methylsulfonyl substituent at R_1 demonstrated an enhanced affinity to *Tb*PEX14 with regard to the parent compound (**10**). The methoxycarbonyl substituent in **11b** afforded a better affinity than the methyl acetate derivative **11a**, which correlated with the increased trypanocidal effect. The analysis of the compound **1**-PEX14 complex structure suggests the possibility of forming more favourable hydrogen bonds with the sidechains of Asp38 and Arg40 in the former compound.

Exchanging the 4-fluorophenyl (**8c**) with phenyl (**8a**) of the R_2 substituent reduced the binding affinity to *Tb*PEX14 and, correspondingly, the trypanocidal activity in the *in vitro* assay. The introduction of heteroatoms in the phenyl portion of R_2 in **8c**, gave the pyridine and the pyrazine derivatives **8k** and **8f**, respectively, which displayed slightly less affinity to *Tb*PEX14 and low trypanocidal activity. The interactions at the Trp pocket are primarily hydrophobic and **8k** and **8f** were tested to evaluate the effect of the less hydrophobic substituents. The introduction of a chlorine in the *meta*- (**8d**) or *para*- (**8e**) position of the benzene ring of R_2 positively influenced the affinity for *Tb*PEX14 compared to the parent compound (**8c**). This can be rationalized considering the length of the C-X bond and the larger size of the Cl compared with F. Although the fluorine atom is more electronegative than chlorine, the chlorine-carbon bond is longer, and hence its dipole moment is more pronounced. Thus, the chlorine in either *meta*- or *para*-positions better supports the van der Waals interactions with the α1 and α3 helices of PEX14. Out of the tested derivatives containing a sulphur atom in the aromatic rings at R_2, the thiazole compound **8h** lacked both the affinity to *Tb*PEX14 and the trypanocidal activity. In turn, the introduction of the thiophene, a classical isostere of the benzene ring in the R_2 residue gave the derivative **8g** with an improved affinity to the target protein compared to the parent compound **8a**. The derivative **8g** displayed an improved trypanocidal activity comparable to the parent compound (**8a**).

The relatively flat SAR in the investigated dibenzo[*b,f*][1,4]oxazepin-11(10*H*)-one derivatives motivated us to modify the linker at R_2 projecting the aromatic residue of the compounds into the Trp pocket of PEX14. An amine and a carbamate were introduced to the linker in **8m** and **8l**, respectively, given the presence of the polar residues around the Trp pocket. Both modifications improved the affinity towards *Tb*PEX14
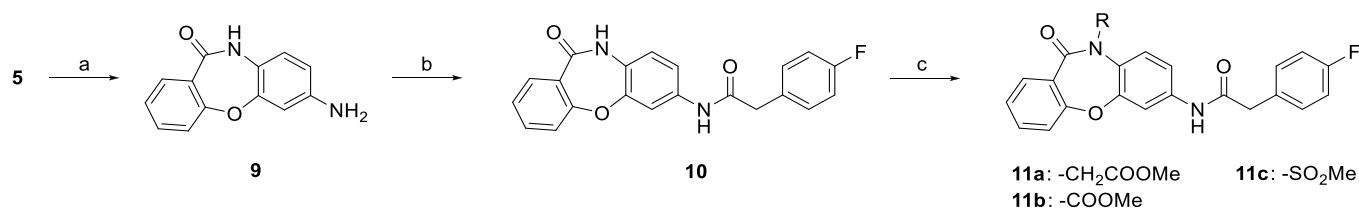
Scheme 3. Synthesis of compounds **11a-c**[a].

compared to the phenyl derivative (**8a**). The introduction of the phenoxycarbonyl residue in **8n** resulted in a significant drop in the trypanocidal activity. The introduction of the methanesulfonyl linker in **8p** yielded a compound with a decreased affinity compared to the phenyl derivative (**8a**) and a decreased trypanocidal potency. The introduction of a sulfonyl moiety in **8o** proved more successful demonstrating an improved affinity towards the target protein compared to the parent compound (**8a**). Importantly, the derivative **8o** was able to kill *Trypanosoma* at low micromolar concentration.

The co-crystal structure of *Tc*PEX14 with compound **1** suggested the possibility of growing the compound deeper inside the Trp pocket. The 1*H*-indol-3-yl, 1*H*-benzo[*d*][1,2,3]triazol-1-yl, and the naphthalen-1yl derivatives, **8i**, **8j** and **8b**, respectively, were evaluated and given the proximity of the polar residues we expected especially favourable interactions of the former two. Indeed, all three compounds were characterized by a significantly higher affinity compared to the parent compound (**8a**) which however has translated only into 2-fold increase in the trypanocidal activity in the case of compounds **8j** and **8b**.

The overall correlation between the trypanocidal activity of the tested derivatives and the affinities towards PEX14 is low (Figure S3) reflecting the complexity of the *in vivo* environment compared to a simple biochemical assay. In the affinity assay PEX14 is directly accessible to the tested compounds while in *Trypanosoma* the compound has to cross the cell membrane, avoid the metabolism and the sequestration by unspecific binding or cellular localization. Moreover, off-target effects of some compounds may not be excluded at this stage.

Overall, this study provided novel PEX14 inhibitors with trypanocidal activity and the initial assessment of the SAR in this class of compounds. Further studies are needed to extend the SAR information at other positions of the scaffold and develop compounds with improved trypanocidal properties.

3. Conclusions

Trypanosomiases are vector-born neglected tropical diseases caused by the infection with the parasitic protists of *Trypanosoma* spp. The lack of safe and effective drugs, especially in the chronic stage of the diseases, and the spreading drug resistance draws the attention to the identification of new molecular targets and inhibitors.

The glycolytic pathway has been suggested as a relevant drug target for the development of novel treatments against trypanosomiases. The unique compartmentalization of the glycolytic enzymes in the glycosomes of the parasite and the large phylogenetic distance to the mammals promises features which could be explored in the design of specific inhibitors. The proof-of-concept has been provided with the successful development of the glyceraldehyde-3-phosphate dehydrogenase inhibitors capable of impeding the growth of *Trypanosoma* parasites *in vitro* [51]. Metabolic enzymes are considered challenging targets *in vivo*, although successful examples have been demonstrated [51,52]. The differential dependence of different lifeforms of *Trypanosoma* on glycolysis further complicates the development. Some of us have earlier explored a novel strategy which targets the glycosomal compartmentalization of multiple metabolic enzymes. The inhibition of the glycosomal transport by blocking the PEX5-PEX14 PPI proved a suitable trypanocidal strategy *in vitro* and *in vivo*. Targeting the glycosome biogenesis and function resulted in metabolic catastrophe and death of *T. brucei* as well as *T. cruzi* parasites [44,53,54]. Building on this knowledge, in this study we provided a new line of PEX14 inhibitors with low micromolar activity against *T. brucei*. The potential trypanocidal activity against *T. cruzi* remains to be tested, but the fact that the compounds provided in this study effectively dissociate *Tc*PEX14-PEX5 interaction allow to expect that at least some may be effective against *T. cruzi* comparably to previously reported PEX14 inhibitors based on different scaffold [44], and despite the differences in the metabolism of the two species.

A single-point AlphaScreen-based HTS allowed to identify the initial

dibenzo[*b,f*][1,4]thiazepin-11(10*H*)-one hits **1** and **2**. The structure of the *T. cruzi* PEX14 NTD in complex with compound **1** revealed the binding pose and the presence of an extended water network supporting the binding [55], and provided the basis for the preliminary SAR exploration in a small sub-set of derivatives. Importantly, our high-resolution X-ray structure revealed a novel chemotype for targeting the PPI interfaces comprising of short helical peptides interacting with the hydrophobic receptor binding pockets with aromatic peptide side-chains. The successful bioisosteric replacement allowed us to bypass the metabolic instability of the dibenzo[*b,f*][1,4]thiazepin-11 (10*H*)-one hits. Driven by the structural information we synthesized a number of active compounds to preliminarily analyze the SAR at two specific regions of the PEX5-PEX14 PPI interface independently: the solvent exposed region and the Trp pocket. The presence of a substituent at the cyclic amide proved critical for the binding, likely by providing interactions with the polar residues in close proximity (e.g. Asp38 and Arg40) or with the aliphatic portion of the Arg40 side chain. The modifications addressing the Trp pocket resulted in improved affinity. In particular, the introduction of bulky substituents, such as indolyl, benzo [*d*][1,2,3]triazolyl, and naphthyl, allowed to efficiently fill the cavity (by the compound stacking between the two helices forming the Trp pocket; compare [44,53]) resulting in higher affinity to *Tb*PEX14, as compared to the parent compound **8c**.

Despite the fact that *Tb*PEX14 and *Tc*PEX14 share high sequence identity and structural similarity, the affinity of tested compounds differed against the two proteins reflecting slightly different design of the binding sites. This demonstrates a challenge for the future design of dual inhibitors.

The correlation between the affinities determined by AlphaScreen and MST was low for certain compounds. Since the assays passed thorough the validation using known inhibitors and inactive compounds the effect may be partly related to unspecific interference by certain compounds, but also to other unknown factors. The source of the often poor correspondence of the trypanocidal activity and the affinity against the target is most likely related to the pharmacokinetic properties (membrane permeability, stability, metabolism and a variety of other factors) of the compounds which were not thoroughly investigated here. Additionally, at this stage, potential off-target effects of certain compounds may not be excluded. The post-translational modifications (PTMs) may have an additional role in determining the differences between the affinity and the trypanocidal activity. The phosphorylation of PEX14 has been reported in several species (*Hansenula polymorpha, Pichia pastoris, Saccharomyces cerevisiae*) [56–65]. It has been shown in *S. cerevisiae* that the phosphorylation of PEX14 provides a mechanism for controlling the peroxisomal import of the citrate synthase 2, which helps adjusting the carbohydrate metabolism according to the nutritional conditions [66]. The effects of the PTMs of the peroxins on the peroxisome biogenesis in *T. brucei* have not been investigated to our knowledge. Yet, the potential PTMs introduce another factor complicating the interpretation of the correlation between the affinity and the trypanocidal activity, since the affinity was determined using the proteins produced in *E. coli* which introduce little PTMs compared to the eucaryotes.

T. cruzi is not reliant on glycolysis for energy generation, yet impairment of glycosomal protein import may still be toxic to *T. cruzi*. Furuya et al. demonstrated that mislocalization of glycolytic enzymes results in metabolic catastrophe in *T. brucei* where uncontrolled glycolysis consumes vital cellular resources resulting in cell death [42]. They furthermore found that it was true for both the bloodstream and the procyclic form of the parasite. Since this latter can grow in the absence of the glucose they concluded that the glycosomal compartmentation may be essential in the other pathogenic trypanosomatids, like Leishmania and *T. cruzi*, which are not exclusively glycolytic. The above, and the fact that another class of PEX14 inhibitors developed in *T. brucei* was effective against *T. cruzi* [44] allow us to speculate that some compounds delivered by this study may show activity against *T. cruzi*. We were unfortunately not able to test this assumption, but

further studies should evaluate the activity of the most promising compounds (**8i,8j,8b**) against *T. cruzi* intracellular amastigotes.

HAT and Chagas disease are significantly different in their chronic stage which has to be addressed in the drug development. *T.cruzi* accumulates primarily in the gastrointestinal tract and in the heart. The drug candidates must be able to cross several barriers before reaching the parasite, while avoiding metabolism, nonspecific binding to the plasma and tissue proteins, etc. With HAT, additional challenge is posed by the blood-brain barrier. In both cases, the optimization of the pharmacokinetics will be very challenging.

In conclusion, we identified a novel scaffold to target the PEX5-PEX14 PPI interaction and provided an initial SAR characteristics. Many of the synthesized inhibitors displayed low micromolar trypanocidal activity in cellular assays against *T.brucei*. The identified scaffold may prove suitable for a more general application in targeting PPIs mediated by short helical protein fragments linking the aromatic pockets. Further investigations within the presented chemotype should seek to i) test the trypanocidal activity against *T. cruzi*, ii) expand the SAR information in other regions of the tricyclic scaffold and iii) address the ADME/PK properties of to identify molecules that may represent preclinical candidates for the development of treatment for neglected tropical diseases related to *Trypanosoma* infections.

4. Experimental section

4.1. General methods

The reagents were purchased from Sigma Aldrich, TCI Europe or Enamine and used without further purification. The dry solvents (THF, DMF, DCM) were purchased from Acros Organics. The Thin Layer Chromatography (TLC) was carried out on Merck TLC Silica gel 60 glass plates. The manual flash column chromatography was performed using Merck Silica gel 60 (particle size 0.040–0.063 mm, 230–400 mesh ASTM). The automated preparative chromatography was performed on a Buchi Reveleris Prep purification system using linear gradient elution and Buchi Reveleris Silica 40 μm cartridges for normal phase (SiO$_2$) or Buchi Reveleris C-18 40 μm cartridges for reverse-phase (RP-C18) separations. The final compounds were ≥95% pure, as determined by HPLC-MS analyses performed on a Dionex UltiMate 3000 HPLC system coupled with a Thermo Scientific ISQ EC-LC (column: Thermo Scientific Accucore RP-MS, 50 × 2.1 mm, particle size 2.6 μm; gradient: water/MeCN containing 0.1% (v/v) formic acid each, 5% MeCN for 0.5 min, 5–95% MeCN over the course of 2 min, 95% MeCN for 4 min, flow rate 0.6 ml/min; UV detection at 254 nm; temperature 20 °C). High resolution mass spectrometry (HRMS) analyses were carried out using a Thermo Scientific Q-Exactive apparatus using an electrospray ionization (ESI). NMR data were recorded on a Varian 300 MHz VNMRS or on a Bruker 600 MHz AV III HD (cryo-QCI) instrument. NMR peaks are reported as follows: chemical shift (δ) in parts per million (ppm) relative to residual non-deuterated solvent and tetramethylsilane (TMS) as the internal standards (CHCl$_3$: $\delta_H = 7.26$, $\delta_C = 77.2$; DMSO: $\delta_H = 2.50$, $\delta_C = 39.5$ ppm), multiplicity (s = singlet, d = doublet, t = triplet, q = quartet, dd = doublet of doublets, ddd = doublet of doublets of doublets, dt = doublet of triplets, td = triplet of doublets, m = multiplet and bs = broad signal), coupling constant (in Hz) and integration.

Compounds **1** and **2** were purchased from Enamine.

2-(4-fluorophenyl)-*N*-(6-isopropyl-11-oxido-5-oxo-5,6-dihydrobenzo[*b*]pyrido[3,2-*f*][1,4]thiazepin-9-yl)acetamide (3). 4.0 mg (0.010 mmol) of **2** was dissolved in 0.2 mL of DCM. A solution of 2.1 mg (0.011 mmol) of *m*CPBA in 0.3 mL of DCM was added dropwise, over 1h. The mixture was quenched with saturated aqueous solution of NaHCO$_3$, washed with 0.5 mL of water, 0.5 mL of brine, dried with anhydrous Na$_2$SO$_4$, filtered and concentrated *in vacuo*. The residue was purified by column chromatography to give 2.2 mg (53%) of the title compound. ^{1}H NMR (600 MHz, DMSO-*d*$_6$) δ 10.59 (s, 1H), 8.64 (d, *J* = 5.1, 1H), 8.09 (d, *J* = 8.4, 1H), 7.97 (s, 1H), 7.67 (d, *J* = 9.1, 1H), 7.54

(dd, *J* = 8.0, 5.2, 1H), 7.51 (d, *J* = 8.8, 1H), 7.34 (t, *J* = 7.1, 2H), 7.13 (t, *J* = 8.8, 2H), 4.75–4.66 (m, 1H), 1.52 (d, *J* = 7.4, 3H), 1.16 (d, *J* = 7.4, 3H). Benzylic -C*H*$_2$- signal overlaps with HDO peak; LC/MS: 438 [M+H]$^+$.

2-Fluoro-*N*-(2-hydroxy-4-nitrophenyl)benzamide (4). 9.72 g (63.05 mmol) of 2-amino-5-nitrophenol was dissolved in 150 mL of dry THF. 17.50 mL (126.10 mmol) of TEA and 0.39 g (3.15 mmol) DMAP were added and the mixture was cooled to 0 °C on an ice-NaCl bath. 7.53 mL (63.05 mmol) of 2-fluorobenzoyl chloride was added dropwise. After 10 min the reaction mixture was allowed to reach room temperature and stirring was continued overnight. The mixture was diluted with distilled water to the final volume of 1000 mL. 2 M aqueous solution of HCl was added until pH of 1. The resulting precipitate was filtered and dried *in vacuo* to give 16.34 g (94%) of yellow solid. The product was used in the next step without further characterization.

7-Nitrodibenzo[*b,f*][1,4]oxazepin-11(10*H*)-one (5). 12.40 g (45.00 mmol) of **4** was dissolved in 150 mL of DMF. Then, 1.80 g (45.00 mmol) of NaOH was added. The mixture was refluxed for 5h. After cooling to room temperature, the reaction mixture was diluted with 500 mL of distilled water. The precipitated solid was filtered, washed with 100 mL of 5% aqueous solution of NaOH and 200 mL of water and dried *in vacuo* to give 8.50 g (73%) of white solid. The product was used in the next step without further characterization.

1-Ethyl-7-nitrodibenzo[*b,f*][1,4]oxazepin-11(10*H*)-one (6). A suspension of 6.00 g (23.40 mmol) of **5** in 150 mL DMF was stirred at 80 °C for 5h. The mixture was cooled to room temperature and 1.34 g (60% dispersion in mineral oil, 35.10 mmol) of NaH was added in small aliquots. The reaction mixture was stirred for 30 min. Subsequently, 17.40 mL (234.00 mmol) of ethyl bromide was added dropwise and the mixture was stirred for 3h. The mixture was poured on 200 mL of ice-water and the resulting cloudy solution was extracted with 3 x 80 mL of DCM, and the combined organic extract was washed with 1 x 100 mL of water, 1 x 100 mL of saturated aqueous solution of NH$_4$Cl, dried with anhydrous Na$_2$SO$_4$, filtered and concentrated in *vacuo*. The resulting crude brown oil 3.39 g (51%) was used in the next reaction without further purification.

7-amino-10-ethyldibenzo[*b,f*][1,4]oxazepin-11(10*H*)-one (7). 6.00 g (21.00 mmol) of crude **6** was dissolved in 100 mL of anhydrous EtOH. Then 14.40 g (84.00 mmol) of anhydrous SnCl$_2$ was added and the mixture was stirred under reflux until TLC (hexane/ethyl acetate 1:1, v/v) showed the completion of the reaction. The mixture was cooled down to room temperature. Water was added, followed by 100 mL of 2 M aqueous solution of NaOH until the pH turned basic. The product was extracted with 2 x 50 mL of DCM/MeOH 8:1 mixture (v/v). The organic phase was washed with 1 x 20 mL of brine, dried with anhydrous Na$_2$SO$_4$, filtered and concentrated *in vacuo*. The residue was recrystallized from DCM to give 3.49 g (65%) of white solid. ^{1}H NMR (300 MHz, DMSO-*d*$_6$) δ 7.67 (dd, J = 7.7, 1.7, 1H), 7.50 (ddd, J = 8.1, 7.4, 1.8, 1H), 7.30–7.17 (m, 2H), 7.13 (d, J = 8.7, 1H), 6.49 (d, J = 2.5, 1H), 6.44 (dd, J = 8.6, 2.5, 1H), 5.33 (s, 2H), 3.97 (d, 2H), 1.17 (t, *J* = 7.0 Hz, 3H); ^{13}C NMR (75 MHz, DMSO-*d*$_6$) δ 165.0, 160.1, 155.6, 147.9, 133.1, 131.3, 127.3, 125.2, 124.0, 121.8, 119.7, 111.3, 105.1, 42.9, 13.4; HRMS (ESI) *m/z*: [M+H]+ calcd for C$_{15}$H$_{14}$N$_2$O$_2$: 255.11280, found: 255.11279.

4.2. General procedure for synthesis of derivatives 8a-k

1.0 eq. of an appropriate starting carboxylic acid was dissolved in DMF (5 mL per 1.0 mmol of acid). Next, 1.2 eq. of HOBt monohydrate, 1.2 eq. of EDC and 4.0 eq. of DIEA were added, followed by 1.0 eq. of **7**. The solution was stirred at room temperature for 3 days. The mixture was diluted with 10 mL of distilled water, transferred into a separatory funnel and extracted with 3 x 10 mL of DCM. The organic phase was washed with 1 x 10 mL of distilled water and 1 x 10 mL of saturated aqueous solution of NH$_4$Cl, dried with anhydrous Na$_2$SO$_4$, filtered and concentrated *in vacuo*. The crude products were purified by the automated reverse-phase (RP-18) flash chromatography (water/MeOH

gradient from 95:5 to 5:95 v/v).

N-(10-ethyl-11-oxo-10,11-dihydrodibenzo[b,f][1,4]oxazepin-7-yl)-2-phenylacetamide (8a). From 80 mg (0.59 mmol) phenylacetic acid, yield: 70 mg (48%).^{1}H NMR (300 MHz, CDCl$_3$) δ 7.80 (dd, *J* = 7.7, 1.8 Hz, 1H), 7.53 (s, 1H), 7.44–7.23 (m, 8H), 7.22–7.09 (m, 4H), 4.10 (q, *J* = 7.1 Hz, 2H), 3.72 (s, 2H), 1.31 (t, 2H); ^{13}C NMR (75 MHz, CDCl$_3$) δ 169.2, 166.10, 160.5, 155.0, 136.0, 134.1, 133.2, 132.0, 130.7, 129.5, 129.3, 127.8, 126.9, 125.3, 123.2, 119.8, 116.8, 112.9, 44.7, 44.1, 13.7; HRMS (ESI) *m/z*: [M+H]$^+$ calcd for C$_{23}$H$_{20}$N$_2$O$_3$: 373.15467, found: 373.15465.

N-(10-ethyl-11-oxo-10,11-dihydrodibenzo[b,f][1,4]oxazepin-7-yl)-2-naphtylylacetamide (8b). From 109 mg (0.59 mmol) of 1-naphthaleneacetic acid, yield: 93 mg (37%). ^{1}H NMR (300 MHz, CDCl$_3$) δ 7.99 (d, *J* = 6.3 Hz, 1H), 7.95–7.84 (m, 2H), 7.78 (d, *J* = 7.7 Hz, 1H), 7.62–7.45 (m, 4H), 7.44–7.32 (m, 2H), 7.22–6.95 (m, 5H), 4.17 (s, 2H), 4.06 (q, *J* = 7.1, 2H), 1.28 (t, *J* = 7.0, 3H); ^{13}C NMR (75 MHz, CDCl$_3$) δ 169.6, 166.5, 160.9, 155.4, 136.2, 134.6, 133.6, 132.5, 132.4, 131.2, 130.8, 129.5, 129.4, 129.0, 127.7, 127.4, 126.9, 126.2, 125.8, 124.0, 123.6, 120.2, 117.4, 113.4, 44.5, 43.2, 14.1; HRMS (ESI) *m/z*: [M+H]$^+$ calcd for C$_{27}$H$_{22}$N$_2$O$_3$: 423.17032, found: 423.17042.

N-(10-ethyl-11-oxo-10,11-dihydrodibenzo[b,f][1,4]oxazepin-7-yl)-2-(4-fluorophenyl)acetamide (8c). From 54 mg (0.35 mmol) of 4-fluorophenylacetic acid, yield: 115 mg (83%). ^{1}H NMR (300 MHz, CDCl$_3$) δ 7.80 (dd, *J* = 7.7, 1.8, 1H), 7.55 (s, 1H), 7.46–7.33 (m, 2H), 7.33–7.23 (m, 2H), 7.22–7.02 (m, 6H), 4.10 (q, *J* = 7.1, 2H), 3.68 (s, 2H), 1.31 (t, *J* = 7.1, 3H); ^{13}C NMR (75 MHz, CDCl$_3$) δ 169.4, 166.6, 162.7 (d, *J* = 245.3, 1C), 160.9, 155.4, 136.4, 133.7, 132.4, 131.5 (d, *J* = 8.0), 131.2, 130.3 (d, *J* = 3.4), 127.4, 125.8, 123.7, 120.2, 117.3, 116.5 (d, *J* = 21.6), 113.4, 44.5, 44.2, 14.2; HRMS (ESI) *m/z*: [M+H]$^+$ calcd for C$_{23}$H$_{19}$FN$_2$O$_3$: 391.14525, found: 391.14541.

2-(3-chlorophenyl)-N-(10-ethyl-11-oxo-10,11-dihydrodibenzo[b,f][1,4]oxazepin-7-yl)acetamide (8d). From 251 mg (1.47 mmol) of 3-chlorophenylacetic acid, yield: 118 mg (49%). ^{1}H NMR (300 MHz, CDCl$_3$) δ 7.83–7.72 (m, 2H), 7.58 (d, *J* = 2.1, 1H), 7.38 (td, *J* = 7.7, 1.8, 1H), 7.33–7.24 (m, 3H), 7.24–7.07 (m, 5H), 4.10 (q, *J* = 7.1 Hz, 2H), 3.66 (s, 2H), 1.32 (t, *J* = 7.1, 3H); ^{13}C NMR (75 MHz, CDCl$_3$) δ 169.0, 166.7, 160.9, 155.4, 136.6, 136.5, 135.3, 133.8, 132.4, 131.2, 130.7, 129.9, 128.3, 128.0, 127.3, 125.8, 123.7, 120.2, 117.4, 113.5, 44.6, 44.5, 14.2; HRMS (ESI) *m/z*: [M+H]$^+$ calcd for C$_{23}$H$_{19}$ClN$_2$O$_3$: 407.11570, found: 407.113600.

2-(4-chlorophenyl)-N-(10-ethyl-11-oxo-10,11-dihydrodibenzo[b,f][1,4]oxazepin-7-yl)acetamide (8e). From 251 mg (1.47 mmol) of 4-chlorophenylacetic acid, yield: 137 mg (57%). ^{1}H NMR (300 MHz, CDCl$_3$) δ 7.80 (dd, *J* = 7.8, 1.7, 1H), 7.54 (t, *J* = 1.4, 1H), 7.44–7.26 (m, 5H), 7.26–7.09 (m, 5H), 4.11 (q, *J* = 7.1, 2H), 3.68 (s, 2H), 1.32 (t, *J* = 7.1, 3H); ^{13}C NMR (75 MHz, CDCl$_3$) δ 133.2, 132.0, 130.8, 129.4, 125.4, 123.3, 119.7, 113.0, 70.48, 65.40, 63.55, 44.32, 44.11, 34.38, 32.14, 29.91, 29.67, 29.58, 29.46, 25.14, 22.91, 14.34, 13.94.; HRMS (ESI) *m/z*: [M+H]$^+$ calcd for C$_{23}$H$_{19}$ClN$_2$O$_3$: 407.11570, found: 407.11603.

N-(10-ethyl-11-oxo-10,11-dihydrodibenzo[b,f][1,4]oxazepin-7-yl)-2-(pyrazin-2-yl)acetamide (8f). From 95 mg (0.67 mmol) of 2-(pyrazin-2-yl)acetic acid, yield: 44 mg (42%). ^{1}H NMR (300 MHz, CDCl$_3$) δ 9.19 (s, 1H), 8.65 (s, 1H), 8.59 (s, 2H), 7.82 (dd, *J* = 7.7, 1.7, 1H), 7.60 (d, *J* = 2.4, 1H), 7.41 (td, *J* = 7.7, 1.8, 1H), 7.31 (dd, *J* = 8.8, 2.4, 1H), 7.26–7.12 (m, 3H), 4.12 (q, *J* = 7.1, 2H), 3.91 (s, 2H), 1.33 (t, *J* = 7.1, 3H); ^{13}C NMR (75 MHz, CDCl$_3$) δ 166.1, 165.9, 160.5, 155.0, 150.6, 145.6, 143.8, 143.4, 135.9, 133.2, 132.0, 130.8, 127.0, 125.4, 123.3, 119.7, 117.0, 113.0, 70.3, 65.2, 63.4, 44.1, 43.1, 34.2, 31.9, 29.7, 29.5, 29.4, 29.3, 29.1, 14.1; HRMS (ESI) *m/z*: [M+H]$^+$ calcd for C$_{21}$H$_{18}$N$_4$O$_3$: 375.14517, found: 375.14536.

N-(10-ethyl-11-oxo-10,11-dihydrodibenzo[b,f][1,4]oxazepin-7-yl)-2-(thiophen-3-yl)acetamide (8g). From 83 mg (0.59 mmol) of 3-tiopheneacetic acid, yield: 157 mg (70%). ^{1}H NMR (300 MHz, CDCl$_3$) δ 7.79 (d, *J* = 7.7, 1H), 7.71 (s, 1H), 7.56 (s, 1H), 7.37 (d, *J* = 6.7 Hz, 2H), 7.24–6.93 (m, 6H), 4.10 (d, *J* = 7.3, 2H), 3.73 (s, 2H), 1.31 (t, *J* = 7.1, 3H); ^{13}C NMR (75 MHz, CDCl$_3$) δ 169.3, 166.6, 160.9, 155.4, 136.5,

134.6, 133.7, 132.4, 131.1, 128.8, 127.5, 127.3, 125.8, 124.2, 123.6, 120.2, 117.4, 113.4, 44.6, 39.5, 14.2; HRMS (ESI) *m/z*: [M+H]$^+$ calcd for C$_{21}$H$_{18}$N$_2$O$_3$S: 379.11109, found: 379.11121.

N-(10-ethyl-11-oxo-10,11-dihydrodibenzo[b,f][1,4]oxazepin-7-yl)-2-(1,3-thiazol-4-yl)acetamide (8h). From 84 mg (0.59 mmol) of 2-thiazoleacetic acid, yield: 166 mg (74%). ^{1}H NMR (300 MHz, CDCl$_3$) δ 9.34 (s, 1H), 8.89 (s, 1H), 7.80 (d, *J* = 7.7, 1H), 7.60 (s, 1H), 7.38 (t, *J* = 7.7, 1H), 7.32–7.08 (m, 5H), 4.10 (q, *J* = 7.3, 2H), 3.92 (s, 2H), 1.30 (t, *J* = 7.0, 3H); ^{13}C NMR (75 MHz, CDCl$_3$) δ 167.6, 166.6, 161.0, 155.4, 154.5, 150.4, 136.7, 133.6, 132.4, 130.9, 127.4, 125.8, 123.6, 120.2, 117.4, 117.0, 113.3, 44.5, 40.0, 14.2; HRMS (ESI) *m/z*: [M+H]$^+$ calcd for C$_{20}$H$_{17}$N$_3$O$_3$: 380.10634, found: 380.10663.

N-(10-ethyl-11-oxo-10,11-dihydrodibenzo[b,f][1,4]oxazepin-7-yl)-2-(1H-indol-3-yl)acetamide (8i). From 103 mg (0.59 mmol) of indole-3-acetic acid, yield: 112 mg (46%). ^{1}H NMR (300 MHz, CDCl$_3$) δ 8.35 (s, 1H), 7.82 (d, *J* = 7.7, 1H), 7.62 (d, *J* = 7.8, 1H), 7.47 (d, *J* = 7.9, 2H), 7.43 (s, 1H), 7.43–7.30 (m, 1H), 7.29 (d, *J* = 6.8, 2H), 7.28–7.05 (m, 4H), 4.10 (d, *J* = 7.2, 2H), 3.92 (s, 2H), 1.32 (t, *J* = 7.1, 3H); ^{13}C NMR (75 MHz, CDCl$_3$) δ 154.9, 133.2, 132.0, 125.3, 124.0, 123.1, 123.0, 120.6, 119.8, 118.6, 116.9, 112.9, 111.6, 44.0, 34.5, 13.7; HRMS (ESI) *m/z*: [M+H]$^+$ calcd for C$_{25}$H$_{21}$N$_3$O$_3$: 412.16557, found: 412.16569.

N-(10-ethyl-11-oxo-10,11-dihydrodibenzo[b,f][1,4]oxazepin-7-yl)-2-(1H-benzo[d][1,2,3]triazol-1-yl)acetamide (8j). From 127 mg (0.59 mmol) of benzotriazol-1-yl acetic acid potassium salt and 1 eq. of 37% HCl$_{aq}$., yield: 56 mg (23%). ^{1}H NMR (300 MHz, DMSO-*d$_6$*) δ 10.81 (s, 1H), 8.08 (d, *J* = 8.4 Hz, 1H), 7.84 (d, *J* = 8.2, 1H), 7.77–7.66 (m, 2H), 7.55 (q, *J* = 8.8, 3H), 7.48–7.36 (m, 2H), 7.28 (d, *J* = 8.4, 2H), 5.70 (s, 2H), 4.06 (d, *J* = 8.8, 2H), 1.21 (t, *J* = 7.0, 3H); ^{13}C NMR (75 MHz, DMSO-*d$_6$*) δ 165.3, 165.1, 160.3, 154.6, 145.5, 137.1, 134.3, 134.1, 132.1, 129.9, 127.9, 127.1, 126.1, 124.4, 120.2, 119.5, 117.3, 112.3, 111.4, 50.9, 43.6, 13.9; HRMS (ESI) *m/z*: [M+H]$^+$ calcd for C$_{23}$H$_{19}$N$_5$O$_3$: 414.15607, found: 414.16522.

N-(10-ethyl-11-oxo-10,11-dihydrodibenzo[b,f][1,4]oxazepin-7-yl)-2-(pyridin-3-yl)acetamide (8k). From 81 mg (0.59 mmol) of 3-pyridylacetic acid, yield: 139 mg (63%). ^{1}H NMR (300 MHz, CDCl$_3$) δ 8.62–8.45 (m, 2H), 8.23 (s, 1H), 7.84–7.70 (m, 2H), 7.62 (d, *J* = 2.3, 1H), 7.44–7.29 (m, 2H), 7.26 (s, 1H), 7.24–7.06 (m, 3H), 4.10 (q, *J* = 7.1, 2H), 3.69 (s, 2H), 1.31 (t, *J* = 7.0, 3H); ^{13}C NMR (75 MHz, CDCl$_3$) δ 168.1, 166.2, 160.5, 155.0, 150.0, 148.5, 137.2, 136.1, 133.3, 131.9, 130.8, 130.5, 126.9, 125.4, 123.9, 123.2, 119.8, 117.0, 113.1, 44.2, 41.4, 13.7; HRMS (ESI) *m/z*: [M+H]$^+$ calcd for C$_{22}$H$_{19}$N$_3$O$_3$: 374.14992, found: 374.15010.

(2S)-2-[(tert-butoxycarbonyl)amino]-N-(10-ethyl-11-oxo-10,11-dihydrodibenzo[b,f][1,4]oxazepin-7-yl)-2-phenyl-acetamide (8l). From 296 mg (1.18 mmol) of (S)–N-Boc-Phg-OH, yield: 231 mg (40%). ^{1}H NMR (300 MHz, CDCl$_3$) δ 8.52 (s, 1H), 7.83 (dd, *J* = 7.8, 1.7, 1H), 7.53–7.32 (m, 7H), 7.26–7.11 (m, 3H), 7.05 (d, *J* = 8.9, 1H), 5.86–5.75 (m, 1H), 5.45 (s, 1H), 4.09 (q, *J* = 7.1, 2H), 1.48 (s, 9H), 1.32 (t, *J* = 7.1, 3H); ^{13}C NMR (75 MHz, CDCl$_3$) δ 168.7, 166.0, 160.4, 154.7, 136.9, 135.8, 133.2, 131.9, 130.7, 129.2, 128.8, 127.4, 126.9, 125.3, 123.0, 119.8, 116.9, 112.9, 80.8, 59.4, 44.1, 28.4, 13.7; HRMS (ESI) *m/z*: [M+H]$^+$ calcd for C$_{28}$H$_{29}$N$_3$O$_5$: 488.21800, found: 488.21837.

(2S)-2-amino-N-(10-ethyl-11-oxo-10,11-dihydrodibenzo[b,f][1,4]oxazepin-7-yl)-2-phenylacetamide (8m). 231 mg (0.47 mmol) of 8l was added to 3 mL of a 4 M solution of HCl in 1,4-dioxane. The resulting solution was stirred at rt for 0.5 h, degassed by passing argon and concentrated *in vacuo*. The resulting solid was partitioned between 5 mL of DCM and 2 mL of saturated aqueous solution of NaHCO$_3$. The organic layer was dried with anhydrous Na$_2$SO$_4$, filtered and evaporated *in vacuo*. Yield: 180 mg (70%). ^{1}H NMR (300 MHz, CDCl$_3$) δ 9.58 (s, 1H), 7.82 (dd, *J* = 7.7, 1.7, 1H), 7.72 (d, *J* = 2.4, 1H), 7.5–7.25 (m, 6H), 7.22–7.05 (m, 3H), 4.66 (s, 1H), 4.12 (q, *J* = 7.2, 2H), 2.11 (bs, 2H), 1.34 (t, *J* = 7.2, 3H); ^{13}C NMR (75 MHz, CDCl$_3$) δ 171.2, 166.1, 160.5, 155.1, 140.2, 135.9, 133.2, 132.0, 130.5, 129.1, 128.4, 127.3, 127.0, 126.8, 125.3, 123.3, 119.8, 116.6, 112.6, 60.2, 44.1, 28.3, 13.7; HRMS (ESI) *m/*

z: [M+H]$^+$ calcd for C$_{23}$H$_{21}$N$_3$O$_3$: 388.16557, found: 388.15635.

4.3. General procedure for synthesis of compounds 8n-p

1 eq. of **7** was dissolved in THF (8 mL per 1.0 mmol of **7**). Subsequently, 1.2 eq. of TEA and 0.05 eq. of DMAP were added. The mixture was cooled down to 0 °C on an ice-NaCl bath and stirred for 30 min. Next, 1.0 eq. of an appropriate acylation agent was added. After 10 min, the reaction mixture was allowed to reach slowly room temperature and was stirred overnight. The mixture was diluted with 25 mL of distilled water and was transferred to a separatory funnel and extracted with 3 x 25 mL of DCM. The combined organic extracts were dried with anhydrous Na$_2$SO$_4$, filtered and evaporated *in vacuo*. The crude products were purified by automated flash chromatography RP-18 cartridge column (water/MeOH gradient from 95:5 to 5:95 v/v).

Phenyl (10-ethyl-11-oxo-10,11-dihydrodibenzo[b,f][1,4]oxazepin-7-yl)carbamate (8n). From 92 mg (0.59 mmol) of phenyl chloroformate, yield: 108 mg (49%). ^{1}H NMR (300 MHz, CDCl$_3$) δ 7.87 (t, *J* = 7.0, 1H), 7.54–7.08 (m, 13H), 7.16 (d, *J* = 8.1, 3H), 4.18 (q, *J* = 7.4, 2H), 1.44 (t, *J* = 7.1, 2H); ^{13}C NMR (75 MHz, CDCl$_3$) δ 165.9, 160.3, 154.5, 151.0, 150.4, 135.6, 135.2, 133.6, 132.2, 129.5, 126.7, 126.5, 125.6, 125.6, 123.2, 121.6, 121.1, 119.7, 44.8, 13.9; HRMS (ESI) *m/z*: [M+H]$^+$ calcd for C$_{23}$H$_{20}$N$_2$O$_3$: 373.15467, found: 373.15472.

N-(10-ethyl-11-oxo-10,11-dihydrodibenzo[b,f][1,4]oxazepin-7-yl)benzenesulfonamide (8o). From 139 mg (0.78 mmol) of benzenosulfonyl chloride, yield: 180 mg (58%). ^{1}H NMR (500 MHz, CDCl$_3$) δ 7.92 (dd, *J* = 2.0, 1.0, 2H), 7.91 (t, *J* = 1.6, 2H), 7.86 (dd, *J* = 7.8, 1.7, 1H), 7.70 (ddt, *J* = 7.9, 7.2, 1.2, 2H), 7.57–7.52 (m, 4H), 7.46 (ddd, *J* = 8.2, 7.4, 1.8, 1H), 7.30–7.24 (m, 2H), 7.04 (dd, *J* = 8.2, 1.2, 1H), 6.93–6.86 (m, 2H), 4.13 (q, *J* = 7.1, 2H), 1.41 (t, *J* = 7.1, 3H); ^{13}C NMR (126 MHz, CDCl$_3$) δ 165.7, 160.0, 154.0, 139.2, 137.3, 134.2, 133.6, 132.2, 131.2, 129.1, 129.9, 128.9, 128.6, 128.6, 126.6, 125.7, 124.9, 122.7, 119.6, 44.9, 13.9; HRMS (ESI) *m/z*: [M+H]$^+$ calcd for C$_{21}$H$_{17}$N$_2$O$_4$S: 393.09035, found: 393.09111.

N-(10-ethyl-11-oxo-10,11-dihydrodibenzo[b,f][1,4]oxazepin-7-yl)-1-phenylmethanesulfonamide (8p). From 150 mg (0.78 mmol) of phenylmethylsulfonyl chloride, yield: 210 mg (65%). ^{1}H NMR (500 MHz, CDCl$_3$) δ 7.83 (dd, *J* = 7.8, 1.7 Hz, 1H), 7.43-7,47 (m, 1H), 7.33–7.23 (m, 3H), 7.26–7.20 (m, 3H), 7.20 (d, *J* = 8.8, 1H), 7.16 (dd, *J* = 8.1, 1.1, 1H), 7.07 (d, *J* = 2.6, 1H), 6.94 (dd, *J* = 8.8, 2.6, 1H), 4.32 (s, 2H), 4.11 (q, *J* = 7.1, 2H), 1.35 (t, *J* = 7.1, 3H); ^{13}C NMR (126 MHz, CDCl$_3$) δ 166.0, 160.3, 155.2, 135.3, 133.4, 132.1, 131.3, 130.8, 129.0, 128.9, 128.2, 126.8, 125.5, 123.7, 119.7, 117.0, 113.00, 58.2, 44.3, 13.8; HRMS (ESI) *m/z*: [M+H]$^+$ calcd for C$_{22}$H$_{20}$N$_2$O$_4$S: 409.12165, found: 409.12138.

7-Aminodibenzo[b,f][1,4]oxazepin-11(10H)-one (9). 0.60 g (2.30 mmol) of **5** was dissolved in 20 mL of anhydrous EtOH. Then, 1.80 g (9.20 mmol) of anhydrous SnCl$_2$ was added. The mixture was stirred under reflux for 4h and cooled to room temperature. 2 M aqueous solution of NaOH was added until the basic pH. The product was extracted with 2 x 10 mL of DCM/MeOH 8:1 (v/v) mixture. The organic phase was washed with 1 x 5 mL of brine, dried with anhydrous Na$_2$SO$_4$, filtered and concentrated *in vacuo*. The crude product was purified by flash chromatography (DCM/MeOH gradient: 99:1 to 95:5 v/v) to give 0.25 g (48%) of the title compound. ^{1}H NMR (300 MHz, CDCl$_3$) δ 10.08 (s, 1H), 7.73 (dd, *J* = 7.7, 1.8, 1H), 7.55 (ddd, *J* = 8.1, 7.4, 1.8, 1H), 7.33–7.20 (m, 2H), 6.81 (d, *J* = 8.5, 1H), 6.50 (d, *J* = 2.4, 1H), 6.37 (dd, *J* = 8.4, 2.5, 1H), 5.16 (s, 2H); ^{13}C NMR (75 MHz, CDCl$_3$) δ 165.6, 159.0, 152.0, 147.0, 133.9, 131.2, 126.3, 125.1, 122.3, 120.6, 119.3, 111.1, 105.7; HRMS (ESI) *m/z*: [M+H]$^+$ calcd for C$_{13}$H$_{10}$N$_2$O$_2$: 227.08150, found: 227.08141.

2-(4-Fluorophenyl)-N-(11-oxo-10,11-dihydrodibenzo[b,f][1,4]oxazepin-7-yl)acetamide (10). 0.75 g (4.86 mmol) of 4-fluorophenyl acetic acid was dissolved in 10 mL of dry DMF. Next, 0.89 g (5.83 mmol) of HOBt monohydrate, 1.12 g (5.83 mmol) of EDC and 3.47 ml (19.45 mmol) of DIEA were added. The mixture was stirred for 1h in room temperature followed by addition of 1.10 g (4.86 mmol) of **9**. Stirring was continued overnight. The mixture was evaporated under *vacuum* and dissolved in 10 mL of ethyl acetate. The organic phase was sequentially washed with 1 x 5 mL of 1 M aqueous solution of HCl, 1 x 5 mL of water, 1 x 5 mL of 2 M aqueous solution of NaOH, 1 x 5 mL of water and 1 x 5 mL brine. The organic phase was dried with anhydrous Na$_2$SO$_4$, filtered and concentrated *in vacuo* to give 1.00 g (55%) of the title compound. ^{1}H NMR (300 MHz, DMSO-d_6) δ 10.44 (s, 1H), 10.27 (s, 1H), 7.81–7.69 (m, 2H), 7.59 (td, *J* = 7.7, 1.8, 1H), 7.41–7.21 (m, 5H), 7.21–7.04 (m, 3H), 3.62 (s, 2H); ^{13}C NMR (75 MHz, DMSO-d_6) δ 169.5, 166.1, 161.8 (d, *J* = 241.5), 159.2, 150.8, 136.9, 134.8, 132.4 (d, *J* = 3.0), 131.9, 131.5 (d, *J* = 8.0), 126.7, 126.2, 125.9, 122.1, 121.1, 117.0, 115.5 (d, *J* = 21.2), 112.4, 42.6; HRMS (ESI) *m/z*: [M+H]+ calcd for C$_{21}$H$_{15}$FN$_2$O$_3$: 363.11395, found: 363.11388.

4.4. General procedure for synthesis of compounds 11a-c

1 eq. of **10** was dissolved in dry DMF (2 mL per 0.5 mmol of 7). 1.5 eq. of NaH (60% dispersion in mineral oil) was added. The mixture was stirred until the effervescence ceased. Next, 5 eq. of appropriate alkyl or acyl halide was added and the mixture was stirred overnight. The mixture was diluted with 10 mL of ethyl acetate and washed 1 x 5 mL of 1 M aqueous solution of HCl, 1 x 5 mL of distilled water, 1 x 5 mL of 2 M aqueous solution of NaOH, 1 x 5 mL of distilled water and 1 x 5 mL of brine. The organic phase was dried with anhydrous Na$_2$SO$_4$, filtered and concentrated *in vacuo*. The compounds were purified by flash chromatography (H/EA 1:2 v/v).

Methyl (7-(2-(4-fluorophenyl)acetamido)-11-oxodibenzo[b,f][1,4]oxazepin-10(11H)-yl)acetate (11a). From 0.39 mL (2.07 mmol) of methyl bromoacetate, yield: 137 mg (75%). ^{1}H NMR (300 MHz, DMSO-d_6) δ 10.37 (s, 1H), 7.80–7.68 (m, 2H), 7.60 (ddd, *J* = 8.2, 7.3, 1.8, 1H), 7.39–7.27 (m, 7H), 7.21–7.10 (m, 2H), 4.69 (s, 2H), 3.74 (s, 3H), 3.64 (d, *J* = 1.2, 3H); ^{13}C NMR (75 MHz, DMSO-d_6) δ 169.8, 169.7, 165.8, 160.4, 161.6 (d, *J* = 240.8), 153.3, 138.6, 134.8, 132.27 (d, *J* = 3.1), 132.2, 131.5 (d, *J* = 8.0), 129.4, 126.2, 125.8, 123.1, 120.6, 117.0, 115.5 (d, *J* = 21.2) 111.9, 52.6, 51.7, 42.6; HRMS (ESI) *m/z*: [M+H]$^+$ calcd for C$_{24}$H$_{19}$FN$_2$O$_5$: 435.13508, found: 435.13520.

Methyl 7-(2-(4-fluorophenyl)acetamido)-11-oxodibenzo[b,f][1,4]oxazepine-10(11H)-carboxylate (11b). From 160 µl (2.07 mmol) of methyl chloroformate, yield: 64 mg (37%). ^{1}H NMR (300 MHz, DMSO-d_6) δ 10.47 (s, 1H), 7.94 (dd, *J* = 7.9, 1.7, 1H), 7.87 (d, *J* = 2.3, 1H), 7.68 (ddd, *J* = 8.2, 7.3, 1.8, 1H), 7.55–7.41 (m, 2H), 7.41–7.29 (m, 4H), 7.22–7.08 (m, 2H), 3.81 (s, 2H), 3.66 (d, *J* = 4.3, 2H); ^{13}C NMR (75 MHz, DMSO-d_6) δ 170.0, 164.1, 161.6 (d, *J* = 241.5), 160.5, 155.5, 153.3, 140.1, 136.4, 133.2, 132.2 (d, *J* = 3.1), 131.49 (d, *J* = 8.1), 129.8, 126.3, 124.3, 124.0, 121.4, 116.8, 115.5 (d, *J* = 21.3), 111.5, 54.9, 42.7; HRMS (ESI) *m/z*: [M+H]$^+$ calcd for C$_{23}$H$_{17}$FN$_2$O$_5$: 421.11943, found: 421.11959.

2-(4-Fluorophenyl)-N-[10-(methanesulfonyl)-11-oxo-10,11-dihydrodibenzo[b,f][1,4]oxazepin-7-yl]acetamide (11c). From 160 µl (2.07 mmol) of methanesulfonyl chloride, yield: 70 mg (38%). ^{1}H NMR (300 MHz, DMSO-d_6) δ 10.48 (s, 1H), 7.96–7.80 (m, 2H), 7.79–7.62 (m, 1H), 7.58 (d, *J* = 8.8, 1H), 7.47–7.30 (m, 5H), 7.21–7.07 (m, 2H), 3.85 (s, 2H), 3.35 (s, 3H); ^{13}C NMR (75 MHz, DMSO-d_6) δ 169.5, 165.1, 161.2 (d, *J* = 240.8), 160.4, 156.0, 140.0, 136.0, 132.5, 131.7 (d, *J* = 3.0), 131.0 (d, *J* = 8.0), 129.5, 126.1, 123.9, 122.6, 120.9, 115.9, 115.0 (d, *J* = 21.2), 111.1, 44.2, 42.2; HRMS (ESI) *m/z*: [M+H]$^+$ calcd for C$_{22}$H$_{17}$FN$_2$O$_5$S: 441.09150, found: 441.09150.

Protein expression and purification. The N-terminal domain of *T. cruzi* and *T. brucei* PEX14 (aa 19–84) were cloned into pETM-11 (EMBL). The plasmids were transformed into *E. coli* BL21. 5 ml of the overnight culture was inoculated in 500 ml of the autoinduction medium [70] supplemented with 50 µg of kanamycin. When the cell density (OD$_{600}$) reached 0.8, the temperature was lowered to 18 °C and the cells were grown overnight. The cells were harvested by centrifugation and dissolved in lysis buffer (50 mM Tris pH 8.0, 300 mM NaCl, 10 mM

β-mercaptoethanol, 20 mM imidazole, 10 mg/ml DNAseI, 1 mM AEBSF) and lysed by sonication. The lysates, clarified by centrifugation, were passed over a Ni-NTA agarose resin (Qiagen, Germany) pre-equilibrated with buffer A (50 mM Tris pH 8.0, 300 mM NaCl, 10 mM β-mercaptoethanol, 20 mM imidazole) and the protein of interest was eluted with the same buffer containing 250 mM imidazole. For the AlphaScreen and MST assays, the concentrated eluates were further purified on a Superdex 75 Hiload 16/60 column (GE Healthcare) in phosphate-buffered saline (PBS). For crystallization, the eluate was mixed at 1:100 M ratio with TEV protease and dialyzed overnight at room temperature against the cleavage buffer (50 mM Tris pH 8.0, 1 mM EDTA, 5 mM β-mercaptoethanol). The protease and the cleaved His-tag were removed by the reverse affinity chromatography. The protein contained in the flow through was further purified by size exclusion chromatography (SEC) using the crystallization buffer (10 mM Tris pH 8.0, 100 mM NaCl, 5 mM β-mercaptoethanol).

AlphaScreen assay. The assay was performed according to the published protocols [44,53] and was used to measure the effective concentration (EC_{50}) values for the PEX5-PEX14 inhibitors. 3 nM N-His-PEX14 was mixed with 10 nM biotinylated PEX5-derived peptide (ALSENWAQEFLA) in PBS supplemented with 5 mg/mL of BSA and 0.01% (v/v) Tween-20. 5 μg/mL of streptavidin donor beads and 5 μg/mL of nickel chelate acceptor beads (PerkinElmer) were added to the mixture. The serial dilutions of the inhibitors were prepared in DMSO and mixed while keeping constant the concentration of DMSO (5%; this concentration was shown to have no effect on the assay readout). The signal was determined according to the bead manufacturer instructions. The data were analyzed using Origin Pro 9.0. The experimental points were interpreted using Hill sigmoidal fitting fixing the asymptotes at the maximal assay signal (no inhibitor added) and 0, respectively.

HTS. The HTS platform consisted of an integrated instrumentation for plate and liquid handling. The experiments were performed using a Sciclone G3 Liquid Handler from PerkinElmer (Waltham, MA) with a Mitsubishi robotic arm (Mitsubishi Electric, Tokyo, Japan, RV-3S11) and a Flexdrop dispenser (PerkinElmer) [71]. The AlphaScreen assay was performed in the white 384-well Optiplates (PerkinElmer, product no. 6007299), and the signals were detected on the EnVision Multilabel Reader (PerkinElmer). The proteins and the beads were diluted in an assay buffer containing 1 × PBS (pH 7.4), 0.5% bovine serum albumin (BSA), and 0.1% Tween-20. The AlphaScreen experiments were performed as follows: (1) 40 μL of protein-peptide mix was dispensed into white 384-well plates using a robotic liquid handler; (2) 0.6 μL of compound stock in DMSO was added into each well using the compound transfer station with a nanoliter head; (3) 10 μL each of streptavidin donor and nickel chelate acceptor beads were added, followed by incubation for 1 h at room temperature in the dark; and (4) the assay results were read using the laser excitation at 680 nm and the emission detected at 520–620 nm in an EnVision 2102 Multilabel Reader (PerkinElmer). The quality and the robustness of the assay was evaluated using Z′ factor above 0.8 and the signal window (SW) above 2.

NMR. The saturation transfer difference experiments were used to confirm the AlphaScreen hits. NMR experiments were recorded at 298 K on Bruker Avance III 600-MHz (^{1}H frequency) equipped with a 5-mm TCI or QCI cryoprobe. The STD spectra were recorded at a concentration of 10 μM *Tc*PEX14, with the final concentration of the compound in the sample at 1 mM. DMSO-d_6 was used for the lock signal. The STD experiments used alternating on- and off-resonance saturation with the water suppression using a double-pulsed-field gradient spin-echo (DPFGSE) watergate W5 double-echo sequence [72,73]. The spectra were compared with a reference containing DMSO-d_6 only. The positive hits were identified comparing the intensity ratio of the ligand signals between the STD experiment and a 1D reference spectrum.

MicroScale Thermophoresis (MST) assay. The assay was used for the determination of the inhibitor binding constants (K_d). *Tb* and *Tc* N-His-PEX14 were labeled with Ni-NTA-ATTO647 (Sigma Aldrich) in the MST buffer containing 50 mM Tris-HCl, pH 7.4, 150 mM NaCl, 10 mM

$MgCl_2$ supplemented freshly with 0.0125% (v/v) Tween 20 and by incubating for 1 h at room temperature in the dark. The molar ratio of protein:label of 2:1 was used, and the preparation was utilized in further steps without purification. The serial dilution of the inhibitor was prepared in DMSO and added to the labeled protein (200 nM). The DMSO concentration was kept constant at 5% (v/v). The samples (in triplicates) were loaded into Monolith NT.115 Standard Treated Capillaries and the MST effect was determined. The K_d values were calculated using MO. Affinity Analysis software.

Crystallization and X-ray structure solution. The purified *Tc*PEX14 NTD was mixed with 10-fold molar excess of the ligand (50 mM solution in DMSO) in the storage buffer (10 mM Tris pH 8.0, 100 mM NaCl, 5 mM β-mercaptoethanol, 3% DMSO) and the mixture was incubated for 1h at room temperature. The excess of the ligand and DMSO was removed by washing the complex with the storage buffer at 4 °C on a 10 kDa-cutoff Centricon concentrator. Prior to crystallization the complex was concentrated to about 30 mg/ml. The initial crystallization trials were set up using the commercial kits and TTP LabTech Mosquito automated crystallization workstation. The hits were successively optimized manually using the hanging drop-vapor diffusion technique. The crystals suitable for testing were transferred into a cryoprotectant solution containing the harvesting solution and 25% (v/v) glycerol and cryo-cooled in the liquid nitrogen. The diffraction data were collected at the European Synchrotron Radiation Facility (ESRF, Grenoble, France) beamline ID29. The best diffracting crystal (2.18 Å) was obtained at room temperature in 0.21 M MgCl₂, 0.1 M Tris pH 8.5, 39% (w/v) PEG 4000. The experimental data were processed using XDS and XSCALE software [74]. The crystal belonged to the space group $P\,1\,2_1\,1$. The Matthews coefficient analysis suggested the presence of two molecules of the complex in the asymmetric unit [75]. The structure was solved by molecular replacement using Phaser [76] with *Tb*PEX14 structure (PDB code: 5AON [77]) as a search model. The analysis of the electron density calculated with ($F_o - F_c$) and ($2F_o - F_c$) coefficients allowed to build the initial model and to unambiguously place the ligand using COOT [78] (Figure S4). The starting model was refined by the iterations of manual and automated refinement using Refmac5 [79]. Throughout the refinement 5% of the reflections were used for the cross-validation analysis [80], and the behavior of R_{free} was employed to monitor the refinement strategy. Water molecules were added using Arp/Warp [81] and subsequently manually inspected. The statistics of data collection and refinement are reported in Table S1.

Trypanocidal activity assay. The trypanocidal activity of the compounds was tested against *T. brucei brucei* bloodstream form (BSF) using the resazurin-based 96-well plate assay. *T. b. brucei* BSF (Lister 427) parasites were grown in HMI-11 medium [82] containing 10% fetal bovine serum (FBS) at 37 °C with 5% CO₂. 1:1 serial dilutions (10 points) were prepared in quadruplicates for each compound in HMI-11 medium (100 μL/well). Additionally, each row contained a well without a compound and one with medium solely as controls. 100 μL of parasite cultures (4×10^3/mL) were inoculated in all wells (except the control with medium alone) so that the final concentration of the parasites was 2×10^3/mL. The plates were incubated for 66h. 25 μL of 0.1 mg/mL resazurin (in Hanks Balanced Salt Solution) was added to each well and further incubated till 72 h timepoint. The reduction of resazurin was detected by following the fluorescence emission at 585 nm (excitation 530 nm) using a Synergy H1 microplate reader. The fluorescence emission of the well containing only the medium was considered as background and subtracted from the fluorescence emission of the other wells; then the percent survival values were calculated setting the fluorescence emission of the well without the compound at "100% survival". The experimental data points were fitted with a non-linear regression using GraphPad (6.04) [83] and the half-maximal inhibitory concentration (IC_{50}) values were derived from the corresponding sigmoidal dose-response curves.

Associated content

Supporting **information.** Crystal structure data collection and refinement statistics for *Tc*PEX14-**1** complex structure, comparison of **1** containing and apo-*Tc*PEX14, metabolic biotransformation of compound **2**, correlation between affinity and activity, F_o-F_c map around compound **1**, *in vitro* trypanocidal activity of compounds against *T. brucei brucei*.

Accession Codes. The coordinates of the crystal structure have been deposited to the RCSB Protein Data Bank under the following accession code: **7QRC** (*Tc*PEX14-**1**).

Author contributions

The manuscript was written through contributions of all authors. All authors have given approval to the final version of the manuscript.

V.N.: protein expression and purification, X-ray crystallography, AlphaScreen and MST assay, compounds synthesis;

P.M., M.M., M.D., S.R and T.F.: compounds synthesis; V.C.K., B.G.T.: trypanocidal activity assay; C.S.: AlphaScreen assay and NMR experiments;

J.D., J.O.: MST assay;

K.S. and K.H.: HTS; G.D., M.D., G.M.P, V.N. – study design, funding acquisition, manuscript preparation.

Declaration of competing interest

The authors declare that they have no known competing financial interests or personal relationships that could have appeared to influence the work reported in this paper.

Data availability

Data will be made available on request.

Acknowledgements

Appendix A. Supplementary data

Supplementary data to this article can be found online at https://doi.org/10.1016/j.ejmech.2022.114778.

References

[1] K. Stuart, R. Brun, S. Croft, A. Fairlamb, R.E. Gürtler, J. McKerrow, S. Reed, R. Tarleton, Kinetoplastids: related protozoan pathogens, different diseases, J. Clin. Invest. 118 (4) (2008) 1301–1310.

[2] WHO *The World Health Report 2002: Reducing Risks, Promoting Healthy Life*, World Health Organization, Geneva, 2002.

[3] D.J.J. Kioy, N. Mattock, Focus: human african trypanosomiasis, Nat. Rev. Microbiol. 2 (3) (2004) 186–187.

[4] M.A. Miles, M.D. Feliciangeli, A.R. de Arias, American trypanosomiasis (Chagas' disease) and the role of molecular epidemiology in guiding control strategies, BMJ 326 (7404) (2003) 1444–1448.

[5] G. Langousis, K.L. Hill, Motility and more: the flagellum of Trypanosoma brucei, Nat. Rev. Microbiol. 12 (7) (2014) 505–518.

[6] M.P. Barrett, R.J.S. Burchmore, A. Stich, J.O. Lazzari, A.C. Frasch, J.J. Cazzulo, S. Krishna, The trypanosomiases, Lancet 362 (9394) (2003) 1469–1480.

[7] P. Büscher, G. Cecchi, V. Jamonneau, G. Priotto, Human african trypanosomiasis, Lancet 390 (10110) (2017) 2397–2409.

[8] V. Jamonneau, H. Ilboudo, J. Kaboré, D. Kaba, M. Koffi, P. Solano, A. Garcia, D. Courtin, C. Laveissière, K. Lingue, P. Büscher, B. Bucheton, Untreated human infections by trypanosoma brucei gambiense are not 100% fatal, PLoS Neglected Trop. Dis. 6 (6) (2012), e1691.

[9] J.R. Franco, P.P. Simarro, A. Diarra, J.G. Jannin, Epidemiology of human African trypanosomiasis, Clin. Epidemiol. 6 (2014) 257–275.

[10] J.R. Franco, G. Cecchi, M. Paone, A. Diarra, L. Grout, A. Kadima Ebeja, P. P. Simarro, W. Zhao, D. Argaw, The elimination of human African trypanosomiasis: achievements in relation to WHO road map targets for 2020, PLoS Neglected Trop. Dis. 16 (1) (2022), e0010047.

[11] J.R. Franco, G. Cecchi, G. Priotto, M. Paone, A. Diarra, L. Grout, P.P. Simarro, W. Zhao, D. Argaw, Monitoring the elimination of human African trypanosomiasis: update to 2016, PLoS Neglected Trop. Dis. 12 (12) (2018), e0006890.

[12] K. Vickerman, Antigenic variation in trypanosomes, Nature 273 (5664) (1978) 613–617.

[13] P.G.E. Kennedy, Clinical features, diagnosis, and treatment of human African trypanosomiasis (sleeping sickness), Lancet Neurol. 12 (2) (2013) 186–194.

[14] S. Patterson, S. Wyllie, Nitro drugs for the treatment of trypanosomatid diseases: past, present, and future prospects, Trends Parasitol. 30 (6) (2014) 289–298.

[15] A.Y. Sokolova, S. Wyllie, S. Patterson, S.L. Oza, K.D. Read, A.H. Fairlamb, Cross-resistance to nitro drugs and implications for treatment of human african trypanosomiasis, Antimicrob. Agents Chemother. 54 (7) (2010) 2893–2900.

[16] E.D. Deeks, Fexinidazole: first global approval, Drugs 79 (2) (2019) 215–220.

[17] V. Kande Betu Ku Mesu, W. Mutombo Kalonji, C. Bardonneau, O. Valverde Mordt, D. Ngolo Tete, S. Blesson, F. Simon, S. Delhomme, S. Bernhard, H. Mahenzi Mbembo, C. Mpia Moke, S. Lumeya Vuvu, J. Mudji E'kitiak, F. Akwaso Masa, M. Mukendi Ilunga, D. Mpoyi Muamba Nzambi, T. Mayala Malu, S. Kapongo Tshilumbwa, F. Botalema Bolengi, M. Nkieri Matsho, C. Lumbala, B. Scherrer, N. Strub-Wourgaft, A. Tarral, Oral fexinidazole for stage 1 or early stage 2 African Trypanosoma brucei gambiense trypanosomiasis: a prospective, multicentre, open-label, cohort study, Lancet Global Health 9 (7) (2021) e999–e1008.

[18] R.T. Jacobs, B. Nare, S.A. Wring, M.D. Orr, D. Chen, J.M. Sligar, M.X. Jenks, R. A. Noe, T.S. Bowling, L.T. Mercer, C. Rewerts, E. Gaukel, J. Owens, R. Parham, R. Randolph, B. Beaudet, C.J. Bacchi, N. Yarlett, J.J. Plattner, Y. Freund, C. Ding, T. Akama, Y.K. Zhang, R. Brun, M. Kaiser, I. Scandale, R. Don, SCYX-7158, an orally-active benzoxaborole for the treatment of stage 2 human african trypanosomiasis, PLoS Neglected Trop. Dis. 5 (6) (2011) e1151.

[19] https://ichgcp.net/clinical-trials-registry/NCT03087955.

[20] Chagas disease in Latin America: an epidemiological update based on 2010 estimates, Releve epidemiologique hebdomadaire 90 (6) (2015) 33–43.

[21] O. World Health, The Global Burden of Disease: 2004 Update, 2008.

[22] P.J. Hotez, M.E. Bottazzi, C. Franco-Paredes, S.K. Ault, M.R. Periago, The neglected tropical diseases of Latin America and the caribbean: a review of disease burden and distribution and a roadmap for control and elimination, PLoS Neglected Trop. Dis. 2 (9) (2008), e300.

[23] M. Navarro, B. Navaza, A. Guionnet, R. López-Vélez, Chagas disease in Spain: need for further public health measures, PLoS Neglected Trop. Dis. 6 (12) (2012) e1962-e1962.

[24] J. Gascon, C. Bern, M.J. Pinazo, Chagas disease in Spain, the United States and other non-endemic countries, Acta Trop. 115 (1–2) (2010) 22–27.

[25] L.E. Echeverria, C.A. Morillo, American trypanosomiasis (Chagas disease), Infect. Dis. Clin. 33 (1) (2019) 119–134.

[26] J.H. Maguire, Trypanosoma, in: S. Gorbach, J. Bartlett, N. Backlow (Eds.), Infectious Diseases, Lippincott Williams & Wilkins, Philadelphia, 2004.

[27] A. Rassi Jr., A. Rassi, J.A. Marin-Neto, Chagas disease, Lancet 375 (9723) (2010) 1388–1402.

[28] F.J. Carod-Artal, American trypanosomiasis, Handb. Clin. Neurol. 114 (2013) 103–123.

[29] J.A. Perez-Molina, I. Molina, Chagas disease, Lancet 391 (10115) (2018) 82–94.

[30] C.J. Malone, I. Nevis, E. Fernández, A. Sanchez, A rapid review on the efficacy and safety of pharmacological treatments for Chagas disease, Trav. Med. Infect. Dis. 6 (3) (2021).

[31] J.A. Castro, M.M. de Mecca, L.C. Bartel, Toxic side effects of drugs used to treat Chagas' disease (American trypanosomiasis), Hum. Exp. Toxicol. 25 (8) (2006) 471–479.

[32] C. Bern, S.P. Montgomery, B.L. Herwaldt, A. Rassi, J.A. Marin-Neto, R.O. Dantas, J. H. Maguire, H. Acquatella, C. Morillo, L.V. Kirchhoff, R.H. Gilman, P.A. Reyes, R. Salvatella, A.C. Moore, Evaluation and treatment of Chagas disease in the United States: a systematic review, JAMA 298 (18) (2007) 2171–2181.

[33] M.C. Field, D. Horn, A.H. Fairlamb, M.A. Ferguson, D.W. Gray, K.D. Read, M. De Rycker, L.S. Torrie, P.G. Wyatt, S. Wyllie, I.H. Gilbert, Anti-trypanosomatid drug discovery: an ongoing challenge and a continuing need, Nat. Rev. Microbiol. 15 (4) (2017) 217–231.

[34] H. Acosta, R. Burchmore, C. Naula, M. Gualdron-Lopez, E. Quintero-Troconis, A. J. Caceres, P.A.M. Michels, J.L. Concepcion, W. Quinones, Proteomic analysis of glycosomes from Trypanosoma cruzi epimastigotes, Mol. Biochem. Parasitol. 229 (2019) 62–74.

[35] P.A. Michels, V. Hannaert, F. Bringaud, Metabolic aspects of glycosomes in trypanosomatidae - new data and views, Parasitol. today 16 (11) (2000) 482–489.

[36] F.R. Opperdoes, P. Borst, Localization of nine glycolytic enzymes in a microbody-like organelle in Trypanosoma brucei: the glycosome, FEBS Lett. 80 (2) (1977) 360–364.

[37] X. Barros-Alvarez, M. Gualdrón-López, H. Acosta, A.J. Cáceres, M.A. Graminha, P. A. Michels, J.L. Concepción, W. Quiñones, Glycosomal targets for anti-trypanosomatid drug discovery, Curr. Med. Chem. 21 (15) (2014) 1679–1706.

[38] P.A.M. Michels, O. Villafraz, E. Pineda, M.B. Alencar, A.J. Caceres, A.M. Silber, F. Bringaud, Carbohydrate metabolism in trypanosomatids: new insights revealing novel complexity, diversity and species-unique features, Exp. Parasitol. 224 (2021), 108102.

[39] S.W. van Weelden, B. Fast, A. Vogt, P. van der Meer, J. Saas, J.J. van Hellemond, A. G. Tielens, M. Boshart, Procyclic Trypanosoma brucei do not use Krebs cycle activity for energy generation, J. Biol. Chem. 278 (15) (2003) 12854–12863.

[40] F.R. Opperdoes, Compartmentation of carbohydrate metabolism in trypanosomes, Annu. Rev. Microbiol. 41 (1) (1987) 127–151.

[42] T. Furuya, P. Kessler, A. Jardim, A. Schnaufer, C. Crudder, M. Parsons, Glucose is toxic to glycosome-deficient trypanosomes, Proc. Natl. Acad. Sci. USA 99 (22) (2002), 14177.

[43] R. Erdmann, Assembly, maintenance and dynamics of peroxisomes, Biochim. Biophys. Acta Mol. Cell Res. 1863 (5) (2016) 787–789.

[44] M. Dawidowski, L. Emmanouilidis, V.C. Kalel, K. Tripsianes, K. Schorpp, K. Hadian, M. Kaiser, P. Maser, M. Kolonko, S. Tanghe, A. Rodriguez, W. Schliebs, R. Erdmann, M. Sattler, G.M. Popowicz, Inhibitors of PEX14 disrupt protein import into glycosomes and kill Trypanosoma parasites, Science 355 (6332) (2017) 1416–1420.

[45] A. PerkinElmer, Practical Guide to Working with AlphaScreen, 2004.

[46] M. Mayer, B. Meyer, Group epitope mapping by saturation transfer difference NMR to identify segments of a ligand in direct contact with a protein receptor, J. Am. Chem. Soc. 123 (25) (2001) 6108–6117.

[47] C. Neufeld, F.V. Filipp, B. Simon, A. Neuhaus, N. Schuller, C. David, H. Kooshapur, T. Madl, R. Erdmann, W. Schliebs, M. Wilmanns, M. Sattler, Structural basis for competitive interactions of Pex14 with the import receptors Pex5 and Pex19, EMBO J. 28 (6) (2009) 745–754.

[48] B. Kuhn, J.E. Fuchs, M. Reutlinger, M. Stahl, N.R. Taylor, Rationalizing tight ligand binding through cooperative interaction networks, J. Chem. Inf. Model. 51 (12) (2011) 3180–3198.

[49] J. Zaucha, C.A. Softley, M. Sattler, D. Frishman, G.M. Popowicz, Deep learning model predicts water interaction sites on the surface of proteins using limited-resolution data, Chem. Commun. 56 (98) (2020) 15454–15457.

[50] W.B. Jakoby, D.M. Ziegler, The enzymes of detoxication, J. Biol. Chem. 265 (34) (1990) 20715–20718.

[51] A.M. Aronov, S. Suresh, F.S. Buckner, W.C. Van Voorhis, C.L.M.J. Verlinde, F. R. Opperdoes, W.G.J. Hol, M.H. Gelb, Structure-based design of submicromolar, biologically active inhibitors of trypanosomatid glyceraldehyde-3-phosphate dehydrogenase, Proc. Natl. Acad. Sci. USA 96 (8) (1999) 4273.

[52] I.W. McNae, J. Kinkead, D. Malik, L.-H. Yen, M.K. Walker, C. Swain, S.P. Webster, N. Gray, P.M. Fernandes, E. Myburgh, E.A. Blackburn, R. Ritchie, C. Austin, M. A. Wear, A.J. Highton, A.J. Keats, A. Vong, J. Dornan, J.C. Mottram, P.A. M. Michels, S. Pettit, M.D. Walkinshaw, Fast acting allosteric phosphofructokinase inhibitors block trypanosome glycolysis and cure acute African trypanosomiasis in mice, Nat. Commun. 12 (1) (2021) 1052.

[53] M. Dawidowski, V.C. Kalel, V. Napolitano, R. Fino, K. Schorpp, L. Emmanouilidis, D. Lenhart, M. Ostertag, M. Kaiser, M. Kolonko, B. Tippler, W. Schliebs, G. Dubin, P. Mäser, I.V. Tetko, K. Hadian, O. Plettenburg, R. Erdmann, M. Sattler, G. M. Popowicz, Structure–activity relationship in pyrazolo[4,3-c]pyridines, first inhibitors of PEX14–PEX5 protein–protein interaction with trypanocidal activity, J. Med. Chem. 63 (2) (2020) 847–879.

[54] V.C. Kalel, P. Maser, M. Sattler, R. Erdmann, G.M. Popowicz, Come, sweet death: targeting glycosomal protein import for antitrypanosomal drug development, Curr. Opin. Microbiol. 46 (2018) 116–122.

[55] E.L. Ratkova, M. Dawidowski, V. Napolitano, G. Dubin, R. Fino, M.S. Ostertag, M. Sattler, G. Popowicz, I.V. Tetko, Water envelope has a critical impact on the design of protein–protein interaction inhibitors, Chem. Commun. 56 (2020) 4360–4363.

[56] M. Komori, J.A. Kiel, M. Veenhuis, The peroxisomal membrane protein Pex14p of Hansenula polymorpha is phosphorylated in vivo, FEBS Lett. 457 (3) (1999) 397–399.

[57] M. Komori, M. Veenhuis, Hansenula polymorpha Pex14p phosphorylated in vivo, Cell Biochem. Biophys. 32 (1) (2000) 283–284.

[58] K. Tanaka, M. Soeda, Y. Hashimoto, S. Takenaka, M. Komori, Identification of phosphorylation sites in Hansenula polymorpha Pex14p by mass spectrometry, FEBS Open Bio 3 (2013) 6–10.

[59] M.A. Johnson, W.B. Snyder, J. Lin Cereghino, M. Veenhuis, S. Subramani, J. M. Cregg, Pichia pastoris Pex14p, a phosphorylated peroxisomal membrane protein, is part of a PTS–receptor docking complex and interacts with many peroxins, Yeast 18 (7) (2001) 621–641.

[60] C.P. Albuquerque, M.B. Smolka, S.H. Payne, V. Bafna, J. Eng, H. Zhou, A multidimensional chromatography technology for in-depth phosphoproteome analysis, Mol. Cell. Proteomics 7 (7) (2008) 1389–1396.

[61] F. Gnad, L.M. de Godoy, J. Cox, N. Neuhauser, S. Ren, J.V. Olsen, M. Mann, High-accuracy identification and bioinformatic analysis of in vivo protein phosphorylation sites in yeast, Proteomics 9 (20) (2009) 4642–4652.

[62] L.J. Holt, B.B. Tuch, J. Villén, A.D. Johnson, S.P. Gygi, D.O. Morgan, Global analysis of Cdk1 substrate phosphorylation sites provides insights into evolution, Science 325 (5948) (2009) 1682–1686.

[63] N. Yachie, R. Saito, N. Sugiyama, M. Tomita, Y. Ishihama, Integrative features of the yeast phosphoproteome and protein–protein interaction map, PLoS Comput. Biol. 7 (1) (2011), e1001064.

[64] S. Oeljeklaus, A. Schummer, T. Mastalski, H.W. Platta, B. Warscheid, Regulation of peroxisome dynamics by phosphorylation, Biochim. Biophys. Acta Mol. Cell Res. 1863 (5) (2016) 1027–1037.

[65] Z. Hu, S. Raucci, M. Jaquenoud, R. Hatakeyama, M. Stumpe, R. Rohr, F. Reggiori, C. De Virgilio, J. Dengjel, Multilayered control of protein turnover by TORC1 and Atg1, Cell Rep. 28 (13) (2019) 3486–3496, e6.

[66] A. Schummer, R. Maier, S. Gabay-Maskit, T. Hansen, W.W.D. Mühlhäuser, I. Suppanz, A. Fadel, M. Schuldiner, W. Girzalsky, S. Oeljeklaus, E. Zalckvar, R. Erdmann, B. Warscheid, Pex14p phosphorylation modulates import of citrate synthase 2 into peroxisomes in Saccharomyces cerevisiae, Front. Cell Dev. Biol. 8 (2020).

[70] F.W. Studier, Protein production by auto-induction in high density shaking cultures, Protein Expr. Purif. 41 (1) (2005) 207–234.

[71] K. Schorpp, K. Hadian, Small molecule screening at helmholtz Zentrum münchen–from Biology to molecules, Comb. Chem. High Throughput Screening 17 (3) (2014) 266–271.

[72] M. Piotto, V. Saudek, V. Sklenár, Gradient-tailored excitation for single-quantum NMR spectroscopy of aqueous solutions, J. Biomol. NMR 2 (6) (1992) 661–665.

[73] M. Liu, X.-a. Mao, C. Ye, H. Huang, J.K. Nicholson, J.C. Lindon, Improved WATERGATE pulse sequences for solvent suppression in NMR spectroscopy, J. Magn. Reson. 132 (1) (1998) 125–129.

[74] W. Kabsch, XDS, Acta Crystallogr D Biol. Crystallogr. 66 (Pt 2) (2010) 125–132.

[75] K.A. Kantardjieff, B. Rupp, Matthews coefficient probabilities: improved estimates for unit cell contents of proteins, DNA, and protein-nucleic acid complex crystals, Protein Sci. 12 (9) (2003) 1865–1871.

[76] A.J. McCoy, R.W. Grosse-Kunstleve, P.D. Adams, M.D. Winn, L.C. Storoni, R. J. Read, Phaser crystallographic software, J. Appl. Crystallogr. 40 (Pt 4) (2007) 658–674.

[77] Y. Watanabe, K. Kawaguchi, N. Okuyama, Y. Sugawara, T. Obita, M. Mizuguchi, M. Morita, T. Imanaka, Characterization of the interaction between trypanosoma brucei Pex5p and its receptor Pex14p, FEBS Lett. 590 (2) (2016) 242–250.

[78] P. Emsley, B. Lohkamp, W.G. Scott, K. Cowtan, Features and development of coot, Acta Crystallogr. D Biol. Crystallogr. 66 (Pt 4) (2010) 486–501.

[79] G.N. Murshudov, P. Skubak, A.A. Lebedev, N.S. Pannu, R.A. Steiner, R.A. Nicholls, M.D. Winn, F. Long, A.A. Vagin, REFMAC5 for the refinement of macromolecular crystal structures, Acta Crystallogr. D Biol. Crystallogr. 67 (Pt 4) (2011) 355–367.

[80] A.T. Brünger, Free R value: a novel statistical quantity for assessing the accuracy of crystal structures, Nature 355 (6359) (1992) 472–475.

[81] R.J. Morris, A. Perrakis, V.S. Lamzin, ARP/wARP and automatic interpretation of protein electron density maps, Methods Enzymol. 374 (2003) 229–244.

[82] H. Hirumi, K. Hirumi, Continuous cultivation of Trypanosoma brucei blood stream forms in a medium containing a low concentration of serum protein without feeder cell layers, J. Parasitol. 75 (6) (1989) 985–989.

[83] GraphPad Prism, 6.04; GraphPad Software, Inc: San Diego, CA, USA.